Please cite this as: Gaffney, V., Baldwin, E., Allaby, R., Bates, M., Bates, R., Finlay, A., Gaffney, C., Hansford, T., Kinnaird, T., Neubauer, W., Löcker, K., Sparrow, T., Trinks, I., Wallner, M. and Ch'ng, E. 2025 The Perils of Pits: further research at Durrington Walls henge (2021–2025), Internet Archaeology 69. https://doi.org/10.11141/ia.69.19

The Perils of Pits: further research at Durrington Walls henge (2021–2025)

Vincent Gaffney, Eamonn Baldwin, Robin Allaby, Martin Bates, Richard Bates, Alex Finlay, Christopher Gaffney, Teri Hansford, Timothy Kinnaird, Wolfgang Neubauer, Klaus Löcker, Tom Sparrow, Immo Trinks, Mario Wallner and Eugene Ch'ng

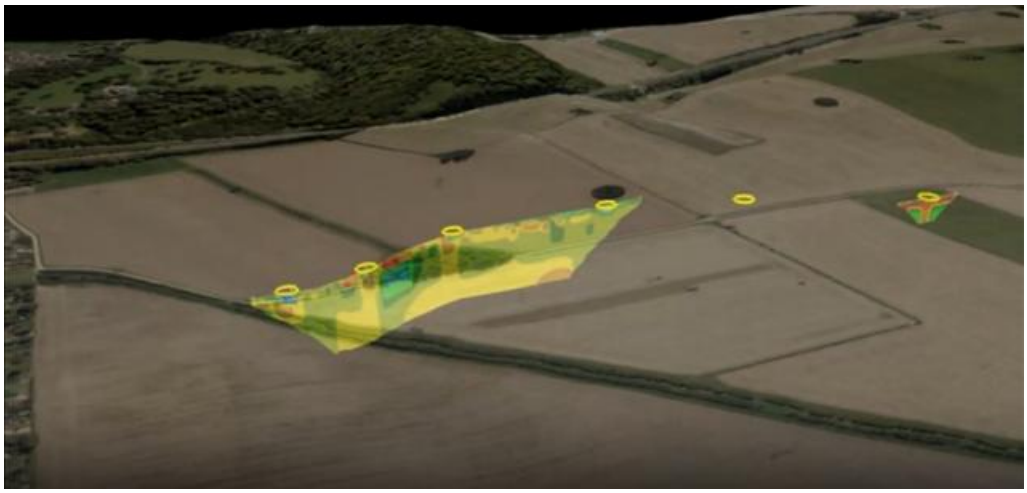

[VIDEO – ONLINE ONLY]

In 2020, a series of large features were identified, set within two arc-like structures, to the north and south of Durrington Walls henge (Gaffney *et al*. 2020). Based on geophysical survey and borehole investigation, combined with the results of previous, commercial fieldwork, 15 features were interpreted as either large pits or probable pits. Five additional features were identified from aerial photography or topographic modelling as being of potential interest. Some of these features, on the 'northern arc', were assessed by their original investigators to be naturally occurring sinkholes (Leivers 2021). Following the interpretation of these features as a single pit alignment, some discussion has taken place relating to the origin and nature of these features and their association with Durrington Walls henge (Ruggles and Chadburn 2024).

This debate has taken place without the benefit of the results of more recent research undertaken both in the field and laboratory. In 2021, further investigations were carried out over 'northern arc' features 13D and 16D, as well as over the 'southern arc' features 1A, 2A, 3A, 4A. This work also provided an opportunity to survey anomaly ii at Larkhill, and to revisit 'southern arc' features 5A, 7A and 8A. The latter three had been surveyed and cored in 2019 and identified as pits. New fieldwork also provided the occasion to utilise a wider range of

analytical techniques than previously, and the application of novel geochemistry and sedaDNA methods generated sediment stratigraphies and detailed environmental histories for individual pits.

The results of geophysical survey and borehole investigations reinforce the overall similarity between those features previously identified as pits or probable pits, as well as those investigated in the recent field campaign. Consequently, with confirmation of pit 16D as a new addition to the 'northern arc', the total of pits/probable pits in the overall series has risen to 16. However, to the west of Durrington Walls, in Larkhill, a magnetometer survey over anomaly ii did not reveal a magnetic response consistent with a large pit-feature, although this area is heavily disturbed by later development and the survey results at this location cannot be regarded as conclusive.

Currently, the majority of features identified during the two seasons of work at Durrington continue to be interpreted as corresponding to large pits or modified features which, irrespective of any possible natural origin, emerged during the later Neolithic to form part of a larger, prehistoric pit structure surrounding Durrington Walls.

1. Introduction

So ferde another clerk with astromye;
He walked in the feeldes, for to prye
Upon the sterres, what ther sholde bifalle,
Til he was in a marle-pit yfalle;
He saugh nat that.
Geoffrey Chaucer, The Millers Tale

In 2020, an extensive arrangement of large features was identified, arranged in two arcs, to the north and south of Durrington Walls, Wiltshire (Gaffney *et al*. 2020). Based on geophysical survey and borehole investigation, combined with the results of previous fieldwork, these features were interpreted as massive pits forming a single structure, centred on the Durrington Walls henge. The pit alignment, with a diameter of more than 2km, was interpreted as an elaboration of the Durrington monument complex at a massive, and unexpected, scale. Constructed during the Late Neolithic, the ring of pits was also shown to incorporate the earlier Larkhill causewayed enclosure in a deliberate manner that suggested a cosmological arrangement. The enlarged monument complex at Durrington, which also represents an important addition to the larger Stonehenge landscape was, significantly, only recognised following the application of remote sensing at a landscape level (Gaffney *et al*. 2012; 2018).

Following publication of the original paper, there has been considerable discussion relating both to the pit structure at Durrington, and also the nature, scale, temporal depth and, perhaps, ubiquity of the practice of pit digging in prehistory (Gaffney *et al*. 2023). Alongside such considerations, there has also been some debate relating to the origin and nature of the Durrington pit group, as well as detailed aspects of the first publication (John 2020; Leivers 2021; Ruggles and Chadburn 2024). Unfortunately, this discourse has occurred without the benefit of results acquired during a second campaign of geophysical and environmental investigation of the pit alignment. Undertaken in 2021, this work was carried out to provide further detail on the character and context of the Durrington pits. The results, presented here, provide a response to the published critique of the original paper. They are also consistent with the original interpretation and indicate that these features formed part of a large, and currently unique, neolithic pit structure surrounding the Durrington Walls henge.

2. Context of the Fieldwork

The geophysical data underpinning this fieldwork was provided as part of the Stonehenge Hidden Landscapes Project. The larger dataset is currently being prepared for publication within a separate volume detailing the results of surveys undertaken primarily between the years 2010–15 (Gaffney *et al*. 2010; 2012; 2018). In autumn 2019 and spring 2020 a limited round of supplementary fieldwork was carried out, prior to publication, to aid the final interpretation of geophysical anomalies of uncertain origin. The interim results for that work were provided in a report for the National Trust in March 2020 (Baldwin and Gaffney 2020). Full results were published in a peer-reviewed article in June of that year (see Gaffney *et al*. 2020).

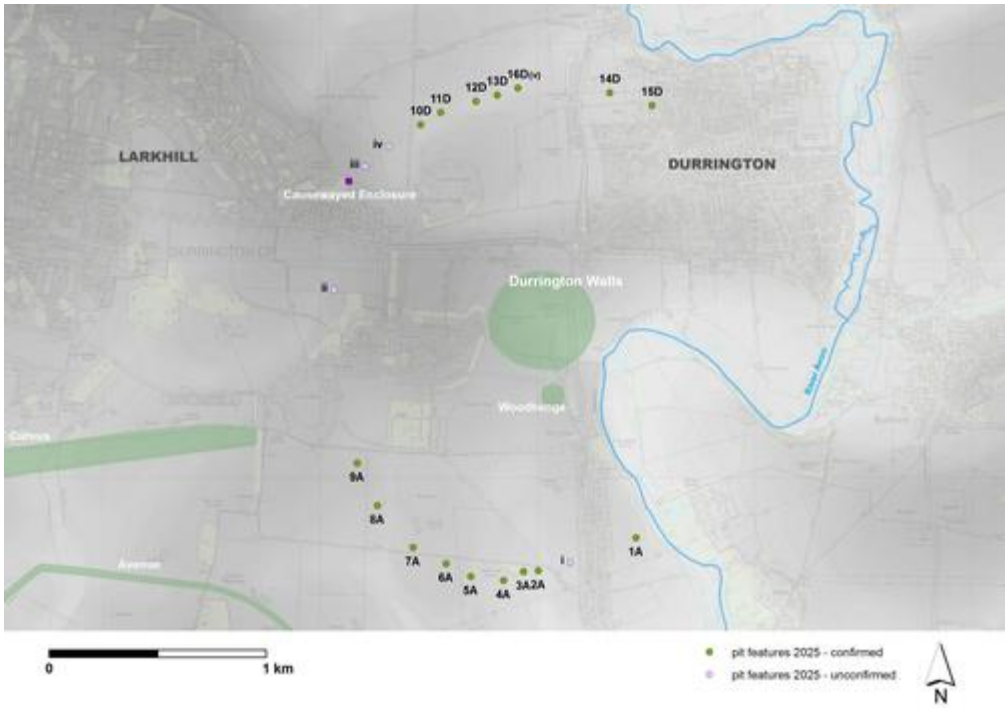

Figure 1: Plan of the pit structure associated with Durrington Walls Henge. Features 1A–9A form an 'arc' south of Durrington Walls in Amesbury parish, while 10D–16D (formerly v) form a northern 'arc' in Durrington parish. Four additional features, noted from other sources including aerial photographs, excavation or topographic modelling, are annotated with roman numerals i–iv. Lidar derived digital surface model (shaded) with OS 10K overlay © Environment Agency copyright and database right 2024. All rights reserved. Lidar (composite sources) DTM 1m resolution, Scale 1:4000 with gaps filled by DTM 2m resolution, Scale 1:8000 – Ordnance Survey (100025252)/EDINA supplied Service. http://digimap.edina.ac.uk

Under investigation in 2019 and 2020 were 15 large, geophysical (pit-like) anomalies; these were identified within the extensive magnetometer data set acquired by the Stonehenge Hidden Landscapes project. These features, numbered 1–15, were apparently aligned in arcs surrounding Durrington Walls henge (see Fig. 1). Anomalies 1–9 have a letter 'A' suffix representing Amesbury parish, while anomalies 10–15 have a letter 'D' suffix representing Durrington parish. Five additional anomalies, tentatively identified from aerial photography, topographic modelling and geophysical survey, were interpreted as possible pit-like features, and were labelled with lower case roman numerals i–v. Investigations in 2019 concluded that anomalies 7A, 8A and 5A were pits and that, by extension, all 15 anomalies were probable pits (Gaffney *et al*. 2020). In spring 2021, permission was granted by the National Trust and the Ministry of Defence for a second round of fieldwork on ten targeted anomalies (1A–5A, 7A, 8A, 13D, and anomalies ii and v), to consolidate the results of the initial study and aid

interpretation of geophysical anomalies before final publication of the Hidden Landscapes project volume. Following the results of survey, and confirmation of anomaly v as a pit made it necessary to rename it 16D, as per the classification outlined above.

Since the initial discovery of these anomalies, by both Wessex Archaeology and the SHLP, six features have been affected by development (iii, iv, 10D, 11D, 14D, 15D). Two of these (iii and 15D) are now totally inaccessible. The other four are now in gardens (iv, 10D), landscaped (11D) or are impacted by new boundaries (14D).

Table 1: Pit features investigated in 2021 and 2019 fieldwork – summary of large pit anomalies
* Not bottomed (≥ at least)
NMP=National Mapping Programme
SHLP=Stonehenge Hidden Landscapes Project
WA=Wessex Archaeology

ID	Parish	Diameter (Upper)	Depth (base)	Dating	Aerial NMP	Geophysics	Borehole	Excavation (partial)	Investigator
Southern 'arc' features									
1A	Amesbury	c.17m	4.7m	MN, BA, EMed	-	Y	Y	-	SHLP
2A	Amesbury	c.15m	≥ 6.7m*	IA	-	Y	Y	-	SHLP
3A	Amesbury	c.17m	6.9m	-	-	Y	Y	-	SHLP
4A	Amesbury	c.17m	-	-	Y	Y	-	-	SHLP
5A	Amesbury	c.20m	≥ 7.0m*	MBA	-	Y	Y	-	SHLP
6A	Amesbury	c.19m	-	-	Y	Y	-	-	SHLP
7A	Amesbury	c.15m	5.0m	LN	Y	Y	Y	-	SHLP
8A	Amesbury	c.18m	5.0m	LN, MBA, IA	-	Y	Y	-	SHLP
9A	Amesbury	c.19m	-	-	Y	Y	-	-	SHLP
Northern 'arc' features									
10D	Durrington	c.22m	≥ 2.0m*	MBA	-	Y	-	Y	WA
11D	Durrington	c.18m	≥ 2.7m*	BA	-	Y	-	Y	WA
12D	Durrington	c.20m	-	-	-	Y	-	-	WA
13D	Durrington	c.15m	4.7m	EN, LN, EBA, LBA, LBA/IA, IA	Y	Y	Y	-	WA/SHLP
14D	Durrington	c.23m	≥ 3.1m*	LN, MBA, RB	-	-	-	Y	WA
15D	Durrington	c.20m	≥ 6.0m*	RB	-	-	Y	Y	WA
16D	Durrington	c.18m	5.8m	LM/EN, EN, LN, EBA, IA, RB	Y	Y	Y	-	SHLP
Potential features									
i	Amesbury	c.20m	-	-	-	Y	-	-	SHLP
iii	Durrington	c.19m	-	-	-	Y	-	Y	WA
iv	Durrington	c.19m	-	-	-	Y	-	Y	WA
Unproven features									
ii	Durrington	c.18m	-	-	Y	Y	-	-	SHLP

3. Aim and Objectives

The primary aim of the 2021 fieldwork, and consequent analysis, was to further characterise those features interpreted as large pits and identified through the application of a range of geophysical and environmental techniques, both invasive and non-invasive (Gaffney *et al*. 2020).

Geophysics objectives:

- Magnetometer survey – to investigate the magnetic response of two possible pit features (anomalies ii and 16D identified from aerial photography or topographic modelling (Gaffney *et al*. 2020), as well as to re-locate the position of 13D (originally magnetic anomaly 6016 as surveyed by Wessex Archaeology, Schmidt and Crabb 2017) for complementary geophysical survey.
- Ground-penetrating radar (GPR), electromagnetic ground conductivity (EM) and electrical resistivity tomography (ERT) and Drone surveys – to investigate further the dimensions, depth and nature of 1A, 2A, 3A, 4A, 5A, 7A, 8A, 13D and 16D, previously identified by Gaffney *et al*. 2020.

Environmental and dating analysis objectives:

- Boreholes – to investigate the depth, composition, age, environmental and depositional sequences of confirmed pits.
- The application of novel analytical techniques including:
    - Chemostratigraphy – to apply geochemical techniques, not usually applied to either terrestrial sediments or prehistoric material, and to test how effective chemostratigraphic techniques are in providing information that might aid the understanding of terrestrial prehistoric deposits,
    - SedaDNA – to determine the ecological composition of the cores, authenticate the presence of ancient DNA and assess for evidence of taphonomic processes.

Ten features were targeted in total. The range of methods applied at each feature in 2021 are summarised in Table 2.

Table 2: Fieldwork undertaken in 2021 with laboratory analyses – progress overview of investigations (previous investigations (P) in 2019 are noted in grey)

Feature	**ii**	**13D**	**16D**	**1A**	**2A**	**3A**	**4A**	**5A**	**7A**	**8A**
Method (field)	Primary targets						Secondary targets			
Magnetometer	X	X	X	P	P	P	P	P	P	P
GPR	-	X	X	X	X	X	-	P	P	P
EM	-	X	X	-	-	-	-	-	P	P
ERT	-	X	X	X	X	X	X	X	X	-
Drone	-	X	X	-	-	-	-	-	-	-
Borehole	-	X	X	X	X	X	-	P	P	P
Analysis (laboratory)										
Core	-	X	X	X	X	X	-	P	P	P
Geochemistry	-	X	X	-	-	-	-	-	-	X
Profiling-OSL	-	X	X	X	X	-	-	X	-	X
Dating-OSL		X	X	X	X		-	-	-	-
aDNA	-	X	X	X	X	X	-	X	X	X
Confirmed pit (interpretation)	?	Yes	Yes	Yes	Yes	Yes	Yes	Yes	Yes	Yes

4. Fieldwork

4.1 Magnetometer Survey

Prior to survey, individual 30m x 30m grids were set out over each target feature with a DGPS unit (Leica GS16 GNSS Rover, Table 3 and Figs 2 and 3). Magnetometry survey within these grids also allowed the accurate targeting of the supporting geophysical and

borehole investigations within individual features. Further methodological details (including post-processing) of the magnetometer surveys are provided in supplementary data file 1.

Table 3: Magnetometer surveys 2021 – summary. March 2021 – Bartington Grad 601 Dual sensor magnetic survey

ID	Survey	Size	Instrument	Transects	Samples	Method
13D	Area	30m x 30m	Bartington Grad 601	1m	25cm	Zigzag
16D	Area	30m x 30m	Bartington Grad 601	1m	25cm	Zigzag
ii	Area	60m x 60m	Bartington Grad 601	1m	25cm	Zigzag

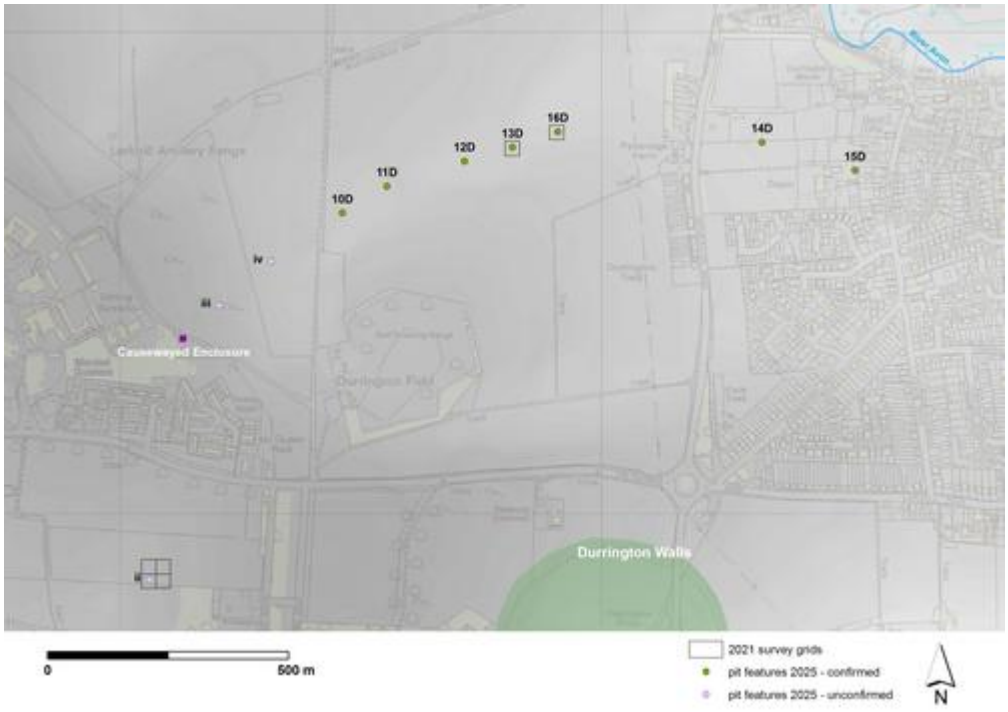

Figure 2: Geophysical survey grid locations for northern anomalies ii, 13D and 16D. These were initially single 30m x 30m grids, although the grid over ii was subsequently expanded to cover an area 60m x 60m. Lidar derived digital surface model (shaded) with OS 10K overlay © Environment Agency copyright and database right 2024. All rights reserved. Lidar (composite sources) DTM 1m resolution, Scale 1:4000 with gaps filled by DTM 2m resolution, Scale 1:8000 – Ordnance Survey (100025252)/EDINA supplied Service. http://digimap.edina.ac.uk

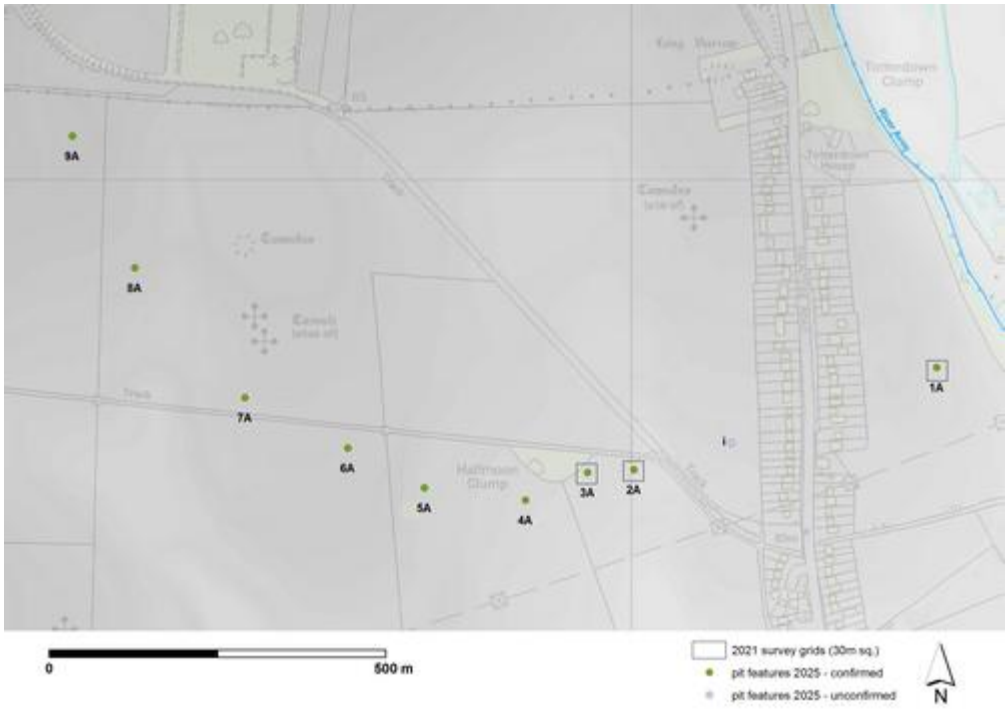

Figure 3: Geophysical survey grid locations for southern anomalies 1A, 2A, and 3A, all single 30m x 30m grids. Lidar derived digital surface model (shaded) with OS 10K overlay © Environment Agency copyright and database right 2024. All rights reserved. Lidar (composite sources) DTM 1m resolution, Scale 1:4000 with gaps filled by DTM 2m resolution, Scale 1:8000 – Ordnance Survey (100025252)/EDINA supplied Service. http://digimap.edina.ac.uk

The results of the magnetic survey (Figs 4–6) were successful in locating all three targets (13D, 16D and ii). Moreover, survey demonstrated that the character and size of cropmark 16D's magnetic response were similar to those anomalies previously identified (1A–9A and 10D–13D, Gaffney *et al*. 2020). Typically, these features are represented by large, sub-circular magnetic anomalies, approximately 18m–20m in diameter. Enhanced, magnetically positive values from within these anomalies suggest structures (natural or anthropogenic) cut into the underlying substrata and then filled with material of a higher magnetic content. Generally, there is a suggestion of a broad 'halo' of less magnetic response surrounding each feature. The results of the magnetic survey brings the sum of probable pit-features to 16 in total.

Following survey, 14 targets, anomalies 1A–9A, 10D–13D, and 16D, have now been identified as pits. primarily based on the consistent character and size of their magnetic response. This interpretation was, in turn, supported by complementary investigations including coring (Gaffney *et al*. 2020). The remaining two features 14D and 15D were identified as being of a similar nature and size, following excavation for mitigation purposes (Gaffney *et al*. 2020; Thompson and Powell 2018).

The magnetic response of 13D had initially been characterised following commercial magnetometry survey (Schmidt and Crabb 2017) and this was reported in Gaffney *et al*. (2020). Reassuringly, the results of the recent survey (albeit at a slightly reduced sample resolution) confirmed the presence of a sub-circular feature *c*.14m in diameter, as mapped in Schmidt and Crabb 2017 (Fig. 3 and included as 13D shown in composite image Fig. 6). The scar of an archaeological watching brief (reported by Leivers *et al*. 2020, Fig. 1) is also evident in the data, running approximately E–W through the southern third of the survey area

in Figure 4. The strong magnetic response from the investigation and backfill overwhelmed some of the weaker magnetic measurements in this area – although it may be noted that a pair of post holes belonging to a late Neolithic post structure were identified running within 7m–10m of 13D during the reported watching brief (Leivers *et al*. 2020, Fig. 6, and included in supplementary data file 1, fig. 1.13).

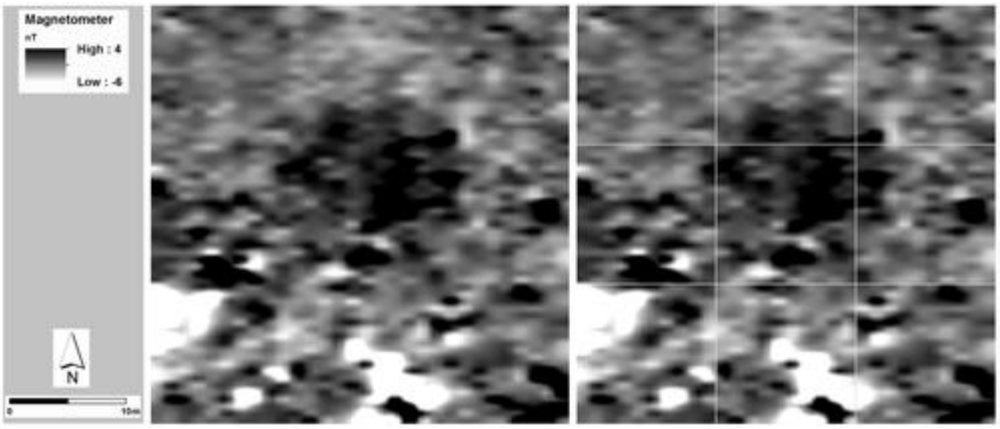

Figure 4: Fluxgate gradiometer survey (30m x 30m) over 13D – processed results at 0.25m x 0.25m spatial resolution (left, and with 10m gridlines right) confirm the location of a previously mapped magnetic anomaly (Schmidt and Crabb 2017, anomaly 6016) approximately 14m in diameter. Greyscale legend: positive (black), negative (white)

The magnetic survey results from 16D successfully located the target feature and also demonstrated a similarity in magnetic response and size to the 15 other magnetic anomalies previously identified as 'pit-like'. Figure 5 illustrates a large sub-circular anomaly approximately 18–20m in diameter. Enhanced readings from within the anomaly again suggest a feature (natural or anthropogenic) cut into the underlying substrata and since filled with material of a higher magnetic content. There is also a suggestion of a broad 'halo' of less magnetic response surrounding the feature.

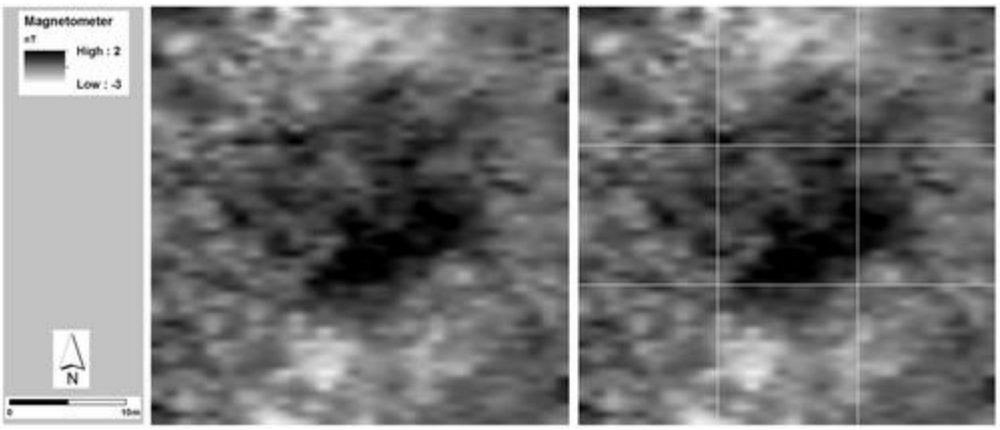

Figure 5: Fluxgate gradiometer survey (30m x 30m) over 16D - identified previously as a cropmark (Gaffney *et al*. 2020) – processed results at 0.25m x 0.25m spatial resolution (left), and with 10m gridlines (right), reveal a previously unmapped magnetic anomaly (approximately 18–20m in diameter, consistent in response and dimension to 15 other pit features identified by Gaffney *et al*. (2020). Greyscale legend: positive (black), negative (white)

Fluxgate gradiometer survey over anomaly ii (Fig. 6) did not, however, detect any magnetic response comparable with other surveyed pit features. Instead, a weakly enhanced rectilinear feature is evident within the survey area. Approximately 15m square, this feature joins, or is cut by, a longer curvilinear feature running through the corner of the survey area NW–SE for over 50m. This feature coincides with the documented line of a perimeter fence that surrounded a WW1 military encampment (Camp 2, see supplementary data file 1, figs 1.5–1.8). Together, these weakly enhanced magnetic responses most probably represent the vestiges of early to mid-20th century military activity. Given the significant disturbance associated with later activity in the area, it was decided that there should be no further investigations at this location. The presence of an earlier feature therefore remains unproven.

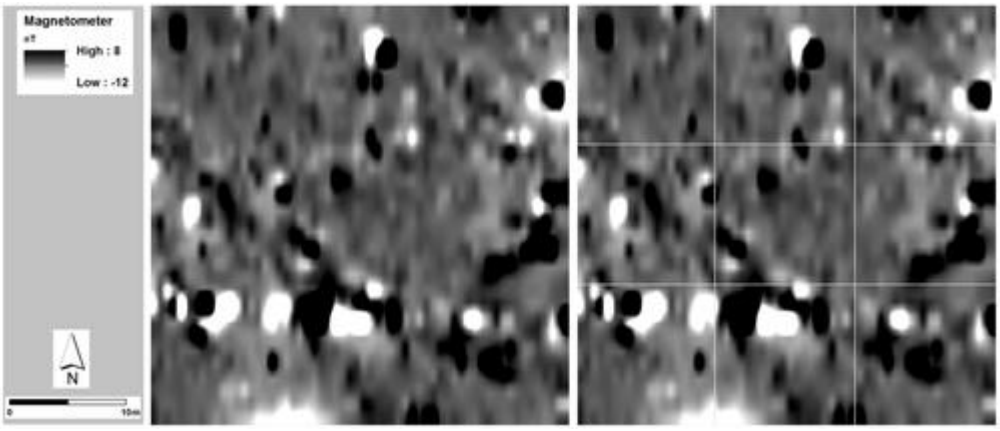

Figure 6: Fluxgate gradiometer survey (30m x 30m grid extracted from a larger area survey – see supplementary data file 1, figs 1.5 and 1.6) over anomaly ii, identified previously as a topographic feature (Gaffney *et al*. 2020) and a cropmark (Crutchley 2002). Processed results at 0.25m x 0.25m spatial resolution (left), and with 10m gridlines (right), reveal a previously unmapped curvilinear magnetic anomaly (approximately 18–20m in diameter), however it is *not* consistent in magnetic response to 15 other pit features (now 16) identified by Gaffney *et al*. (2020), and most probably relates to 20th century military activity in the area. Greyscale legend: positive (black), negative (white)

The results of the magnetometer survey carried out in 2021 are illustrated in Figure 7, along with plans of other features identified as pits from remote sensing or excavation. The similarity across the group suggested that 13D and 16D should be targeted for further geophysical survey and borehole investigation.

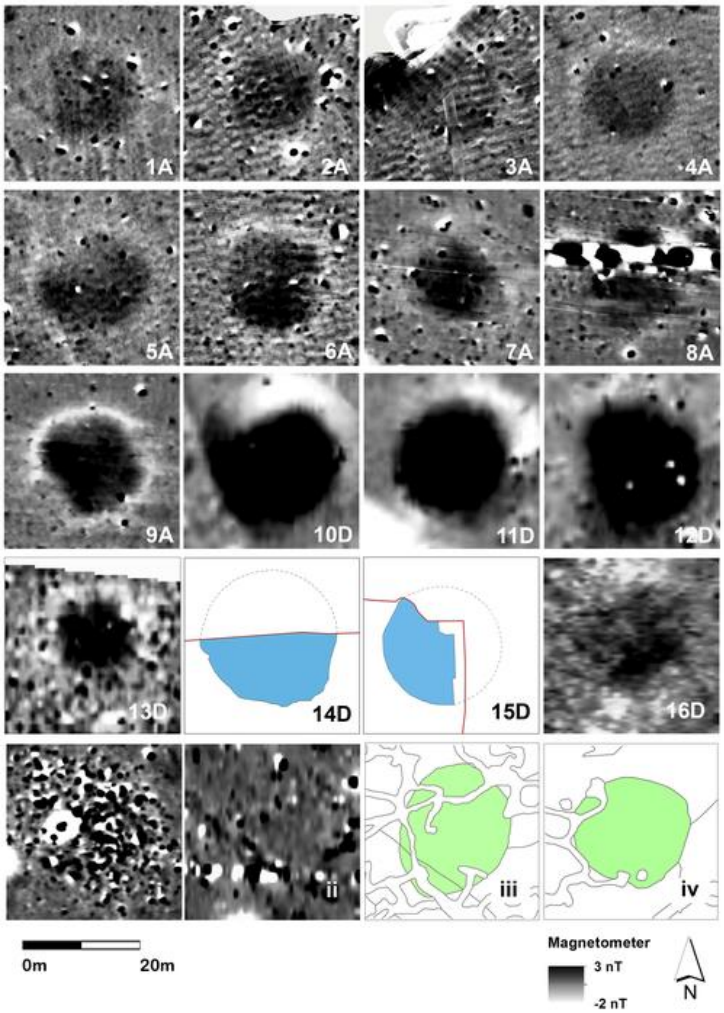

Figure 7: Composite image of 14 magnetic anomalies (1A–9A, 10D–13D and 16D) of similar magnetic character and size. Features 14D and 15D were documented through excavation and are of similar nature and size to the magnetic anomalies. Potential features i, iii, iv remain to be proven. Although similar in size, magnetic anomaly ii displays a dissimilar magnetic characteristic to the others

4.2 Ground Penetrating Radar Survey – GPR

Table 4: GPR surveys 2021 summary. Favourable ground surface conditions (dry, stone free) for cart-mounted GPR survey permitted closer sampling intervals over 2A and 3A.
Fieldwork 2021 – Mala GeoScience X3M single-channel GPR system

ID	Survey	Size	MHz	Transects	No.	Sampling
1A	Area	30m x 30m	250	N–S	61	0.5m x 0.05m
2A	Area	30m x 30m	250	N–S	120	0.25m x 0.05m
3A	Area	30m x 30m	250	N–S	120	0.25m x 0.05m
13D	Area	30m x 30m	250	E–W	61	0.5m x 0.05m
16D	Area	30m x 30m	250	E–W	61	0.5m x 0.05m

Single-channel GPR surveys using a 250MHz antenna were conducted over 1A, 2A, 3A, 13D, and 16D, not only to locate and describe the features in each area (presented as horizontal time-slices), but also to provide additional depth information in profile (presented as vertical radargrams). A time slice summary for each feature is given in Figure 8. A full range of time slices, at increasing depth, for each survey target, can be viewed

in supplementary data file 2, alongside their radargram profiles. As ground surface conditions at 1A, 13D and 16D were poor owing to mud or stoney ground, traverse spacing was limited to 0.5m intervals. Further methodological details of the five single-channel GPR surveys are also provided in the supplementary data file.

Unfortunately, poor weather impacted the GPR survey over 13D and very little subsurface detail was revealed. As a result of near-continuous rain, penetration of the GPR signal was attenuated and it is believed that the imagery reflects the variation in surface covering and not subsurface features. Despite this, the faint (low amplitude) outline of a circular feature, about 25m in diameter, can be seen in the uppermost time slices (Fig. 8, 13D), and there is a hint of a cut into the chalk when viewed in radargram profile 1990 (see supplementary data file 2, fig. 2.3). These data are, however, extremely noisy and, alongside the impact of ploughing, the results may also reflect external electronic interference.

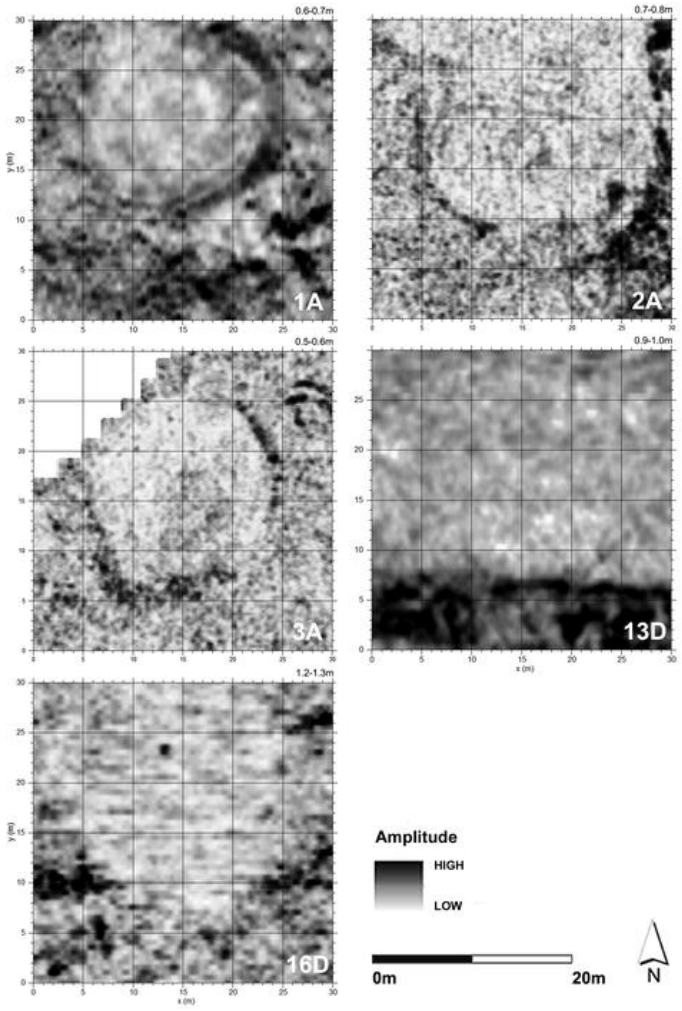

Figure 8: GPR time slices from 1A, 2A, 3A, 13D, and 16D, ranging between an estimated 0.6m–1.3m depth, with 5m grid line intervals marked. North top. Greyscale: high amplitude – black, low amplitude – white

The GPR data over 16D also revealed very little subsurface detail. Once again this resulted from the heavy and continuous rain encountered during survey. However, despite limited penetration, a low-amplitude ovate feature measuring *c*.20–25m in diameter is discernible against the underlying geological response, at time slice depths of *c*.0.6 –1.5m (Fig. 8, 16D). This is also traceable in profile, e.g. radargram 2068 in the supplementary data file 2, figure

2.6. Given the size of the anomaly, it is suggested that this may be interpreted as a weathering cone, above a deeper, cut feature. Similar profiles have been suggested for other pits where GPR results were clearer e.g. 8A (Gaffney *et al*. 2020, table 2.5, supplementary data file 2).

Weather conditions improved considerably during survey over 1A but the soil at this location was stoney and had recently been tilled. Consequently, survey traverse spacing was kept to 0.5m. However, the ground was dry enough to provide a clear GPR signal from survey over the feature.

The time slice in Figure 8 (1A) identifies an elliptical feature directly beneath the topsoil. The GPR data indicate an identifiable weathering cone with a near-circular central feature. Unusually, the near surface plough marks are seen at depth throughout the time slices and presumably are a result of 'ringing' resulting from heavy rain. The presence of a weathering cone and central feature are also discernible in profile (radargram 2130 in the supplementary data file 2, fig. 2.9). A reflective horizontal layer is evident within the weathering cone, effectively 'sealing' the central feature beneath. Deeper again, at *c*.2m depth, the trace of a central, cut feature, *c*.11–12m in diameter, can be seen against the geological background. Unfortunately, the bottom of the feature is not identifiable within the data.

Better ground surface conditions (drier, stone free) permitted a survey interval of 0.25m over 2A and 3A. At 2A, the results reveal a slightly irregular elliptical feature, *c*.20m in diameter and cutting into the underlying geology to an estimated depth between *c*.0.6m–1.2m (Fig. 8, 2A). This seems to be decreasing in diameter with depth, indicating possible modification or erosion through natural processes (see supplementary data file 2, fig. 2.10).

Although the weather conditions were relatively dry during the survey, a combination of recent rain and the high clay content of the underlying subsoil may have limited the penetration of the radar signal. Radargram profile 8815 indicates a significant interface (change in material causing a highly reflective layer response) within the cut of a central feature at *c*.2.2–2.8m depth (see supplementary data file 2, fig. 2.12). The time slice data also suggests a disturbance located centrally within the feature at an estimated depth of *c*.2.2m–2.7m. It is not clear, however, if these responses reflect natural or anthropogenic features. The bottom of the feature is not identifiable in the GPR data or is beyond the limit of detection for the 250MHz antenna.

The results over 3A reveal a distinctly ovate feature (*c*.20m in diameter) cutting into the underlying geology, to an estimated depth of between *c*.0.4m–1.3m (Fig. 8, 3A). This feature seems to decrease in diameter with depth, suggesting the presence of an erosion cone. A combination of recent rain and the high clay content of the underlying geology may have limited the penetration of the radar signal. The base of the feature is not identifiable in the data or is beyond the limit of detection for the 250MHz antenna. Nonetheless, radargram 8711, suggests some deeper responses are discernible in the GPR profile down to *c*.2.5m (supplementary data file 2, fig. 2.15).

In summary, the GPR surveys were successful in providing supporting evidence for all five features surveyed. However, responses were usually limited to a relatively shallow depth (*c*.0.3m–1.5m depth), and the dimension of the recorded features, *c*.18–20m in diameter, suggest that the survey results probably represented the weathering cones of deeper features. Where ground and weather conditions were more conducive to survey, as at 1A, 2A, and 3A, the data also indicated the presence of a narrower, central feature with diameter of *c*.8–12m. Unfortunately, the loss of meaningful response after *c*.3m meant that the GPR was unable to detect the bottom of any of these features (Table 5).

Table 5: Summary of dimension (avg.) as discerned by technique (invasive and non-invasive) undertaken by the Stonehenge Hidden Landscapes project and Wessex Archaeology 2012–2025 (values based on full Table 6.3 in supplementary data file 6)

Technique	Number Investigated	Avg. diameter upper (m)	Avg. diameter lower (m)	Avg. base depth (m)
Magnetometer	14	18		
EM	4	18		
GPR	8	21	12	
ERT	7	20	8	5
Bore hole	9			5
Excavation (partial)	4	21	7	
Avg. Dimensions		**20m**	**9m**	**5m**

4.3 Electromagnetic Ground Conductivity Survey

During 2021, Electromagnetic (EM) ground conductivity measurements were acquired over pits 13D and 16D, using the Geonics EM38 (Table 6). Pits 7A and 8A were surveyed in 2019 using the CMD Explorer. The EM38 was used predominantly in the horizontal mode to record ground conductivity to depths of approximately 0.4m. Further methodological details of all EM surveys are given in supplementary data file 3.

The survey results indicated a variation in conductivity from 2-34mS/m. At 13D (Fig. 9) there were no consistent patterns of conductivity change at the location of the anomaly. Higher values associated with a linear feature crossing the site coincide with a previously unmapped modern feature in the topsoil. This probably relates to recent archaeological investigations (Leivers *et al*. 2020), and also is noted in the Drone survey (see supplementary data file 5).

Table 6: Electromagnetic surveys 2021 summary. March 2021 Fieldwork

ID	Type	Line spacing	Instrument	Sensors	Frequency	Phase	Depth
13D	Area	1m	Geonics EM38	2	0.3hz	quad	c.0.4m
16D	Area	1m	Geonics EM38	2	0.3hz	quad	c.0.4m

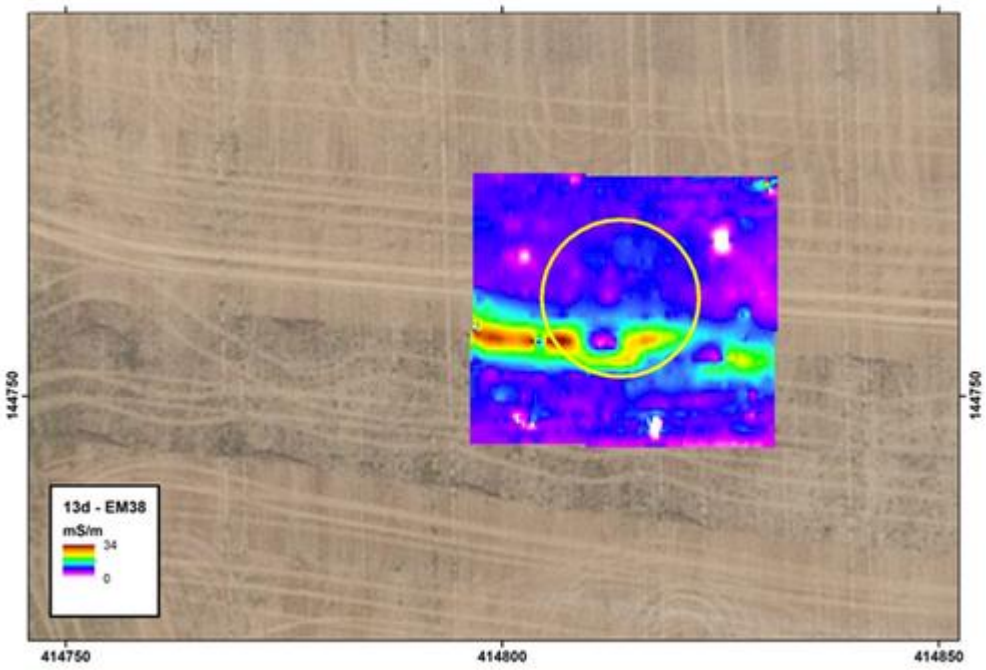

Figure 9: Deployment of the EM38 conductivity meter over 13D showed conductivity variation of 2-34mS/m with high values associated with an E–W trending linear most likely associated with recent archaeological investigations (Leivers *et al*. 2020). No signature was associated with the target location. Backdrop © Google Earth

Results at 16D showed a variation in conductivity of 1-16mS/m. Small spot anomalies (less than 1m size) were randomly scattered throughout the area and a zone of higher ground-conductivity (lower resistivity) was observed both to the north of the anomaly and, approximately, over the location of the anomaly itself (Fig. 10).

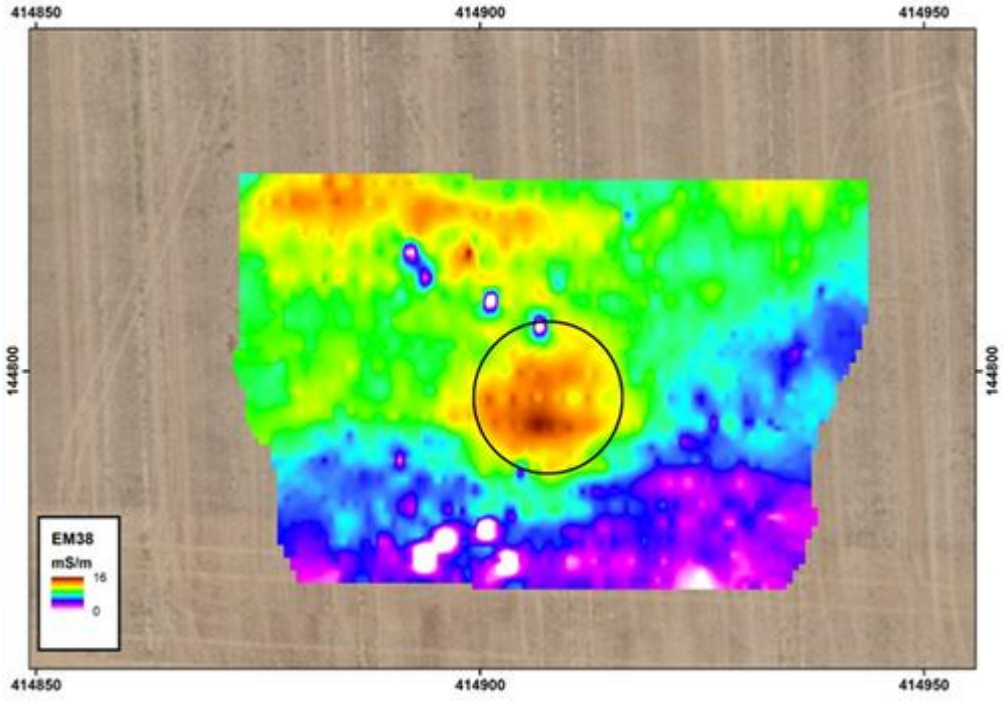

Figure 10: Deployment of the EM38 conductivity meter in horizontal mode over anomaly 16 showed a pattern of generally increasing ground conductivity from south to north across the survey area (top). There was a consistent pattern of higher ground-conductivity associated with the target location (circled). Backdrop © Google Earth

The CMD Explorer ground conductivity meter was also used in horizontal orientation to record both ground conductivity and inphase (magnetic susceptibility) components of the electromagnetic signatures to a maximum penetration of approximately 4m. The results of the survey are shown in supplementary data file 3. A linear feature at Pit 8A, associated with a known water pipe, manifest as a zone of decreased conductivity running east–west, was noted in all three coil separations (near surface to deep) but no signature was noted that coincided with the location of the magnetometer signal (supplementary data file 3, fig. 3.3). The inphase data also showed no patterns that could be related to the location of the magnetometer anomalies. Similar results were returned from survey over 7A (supplementary data file 3, fig. 3.4).

4.4 Electrical Resistance Tomography Survey

Electrical Resistance Tomography (ERT) survey was undertaken with the Flash 64 and ABEM SAS4000 Terrameter with variable electrode spacings – 0.5m, 1m, 2m, and 3m as shown in Table 7. Long-line survey lines were extended using a roll-a-long method involving an overlap of measurements, thereby increasing the length of the line. Data were processed

with Res2DInv software, allowing the generation of electrical pseudo-section models and the topographic correction of long-line ERT transects. Further methodological details are provided in supplementary data file 4, while the locations of long-line ERT transects in relation to the 16 confirmed pits are illustrated in supplementary data file 4, figure 4.14.

Table 7: Electrical Resistance Tomography surveys – 2021 summary

ID	Type	Instrument	Electrodes	Interval (m)	Line Length (m)
13D	Single line	Flash 64	64	1	63
16D	Long line	ABEM SAS4000	64	3	291
1A	Single line	Flash 64	64	1	63
2A	Long line	ABEM SAS4000	64	1	78
5A	Long line	ABEM SAS4000	64	1	78
	Long line	ABEM SAS4000	64	2	156
7A	Long line	ABEM SAS4000	64	0.5	74
	Long line	ABEM SAS4000	64	1	77
5A, 4A, 3A, 2A	Long line	ABEM SAS4000	64	3	408

At 13D, a single ERT line (spacing 1m) was surveyed across the presumed pit (Fig. 11). In the near surface there is a thin, low resistivity layer imaged to depths of less than 1m along the length of the line. Over the presumed pit, a low resistivity feature increases in depth to approximately 4m. Despite the similarity in resistivity of these two regions, it is difficult to confirm (without excavation) if the lower infilling is topsoil derived. The low resistivity signatures do, however, contrast with the higher resistivity layer that also increases in depth over the pit location. The shape of the anomaly is rather amorphous, with a gentle dip to the sides.

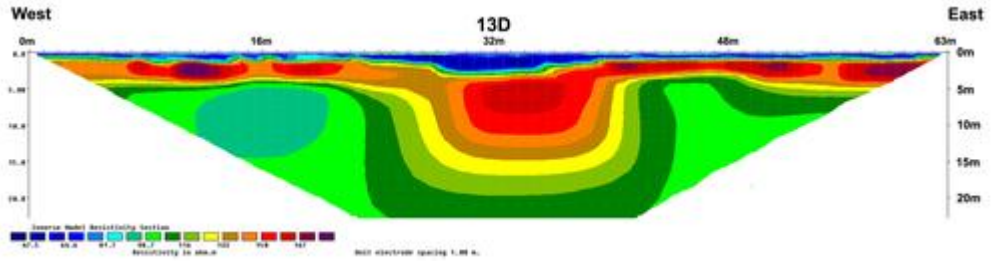

Figure 11: ERT profile across 13D (1m electrode spacing) – a low-resistivity signal located centrally within the profile coincides with the location of 13D. The bottom of the anomaly appears to be at a depth of 4–5m. Colour legend: high resistivity (dark red), low resistivity (dark blue).

At 16D, a relatively long ERT survey line, with an electrode spacing of 3m, was laid north–south, across a shallow valley and through the centre of the feature. This coarser resolution resulted in a slightly poorer definition across the target feature. However, as the intention was to view the pit in context, the results successfully indicated that the pit response is anomalous throughout the section. Figure 12 (top) shows the pseudo-section with penetration to >30m beneath the ground surface. Electrical resistivity values were modelled with a range of resistivity values from 20-300ohmm. The near-surface resistivity values are consistent with the surface, electromagnetic derived ground conductivity, showing a general low conductivity (higher resistivity) area to the south with an increase in conductivity (lower resistivity) in the centre of the valley and immediately to the north of 16D (Fig. 12, below).

Given the 3m electrode spacing utilised, the thin surface present at 16D and described above, was not imaged here. However, the location of the anomaly is coincident with a zone of relatively lower resistivity that is consistent with both the size (*c*.20m in diameter) and depths (*c*.5m) of known pits in both the northern and southern arcs (Gaffney *et al*. 2020).

Again, the profile of the low-resistivity zone, with a flat base and dipping sides, is also comparable with those other features interpreted as pits in Gaffney *et al*. 2020. Furthermore, there is no evidence for changes in resistivity, either below the known features or at any point along the section, that would suggest the presence of structures, such as sinkholes, that might disrupt the continuity of the geological strata at depth.

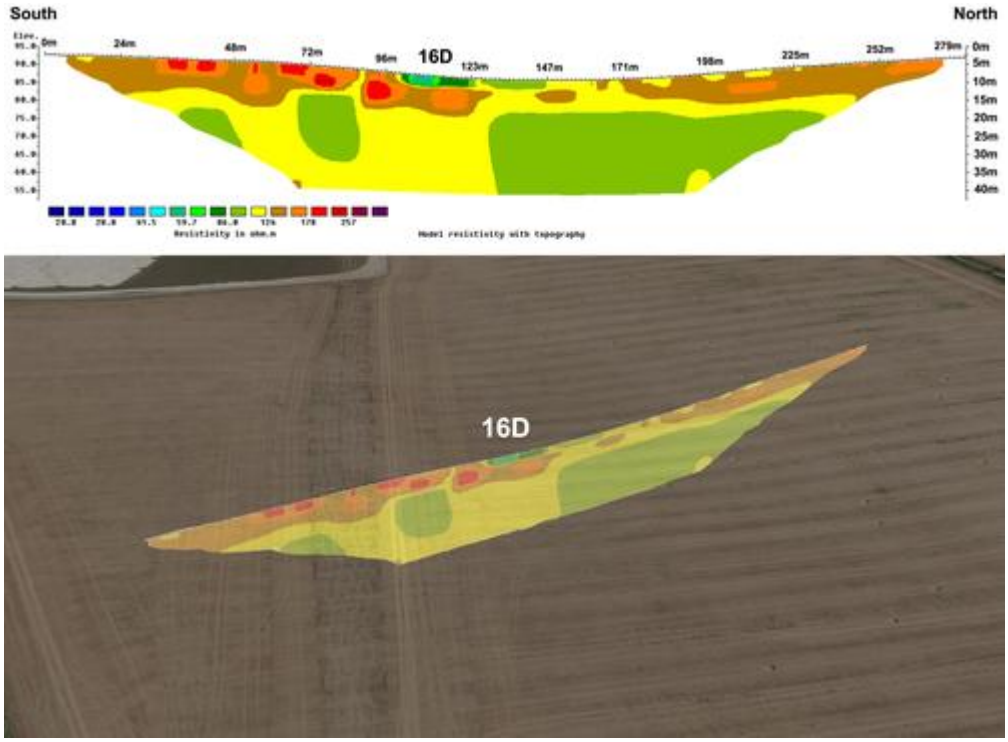

Figure 12: (Top) Vertical ERT profile (3m electrode spacing with topography) running south–north across the dry valley and through 16D – (bottom) the same long-line ERT profile visualised at landscape scale. Colour legend: high resistivity (dark red), low resistivity (dark blue). Backdrop © Google Earth

An ERT line with 1m electrode spacing was also placed across 1A. The centre of the feature was marked by a low resistivity zone of approximately 8m width with relatively steep sides (Fig. 13). The base is marked by an abrupt increase in resistivity at approximately 4.5m depth. At depths over 5m the model shows small contrasts in resistivity along approximately vertical boundaries. However, given the electrode spacing, the model results at these depths are based on relatively few data points and caution is advised when attempting interpretation.

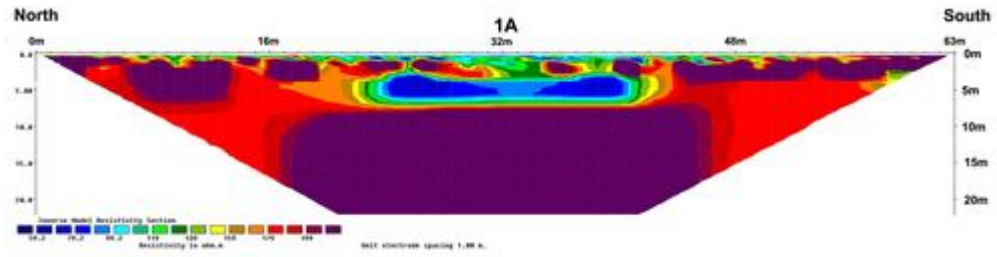

Figure 13: ERT profile across 1A (1m electrode spacing, north–south) – a low-resistivity signal located centrally within the profile coincides with the location of 1A. The bottom of the

anomaly appears to be at a depth of <5m. Colour legend: high resistivity (dark red), low resistivity (dark blue)

ERT results from 2A, acquired with an electrode spacing of 1m, contain a zone of disrupted resistivity that contrasts with the surrounding area (Fig. 14). Here the magnitude of contrast is less than across other anomalies surveyed. The disrupted area is approximately 20m wide and less than 5m deep.

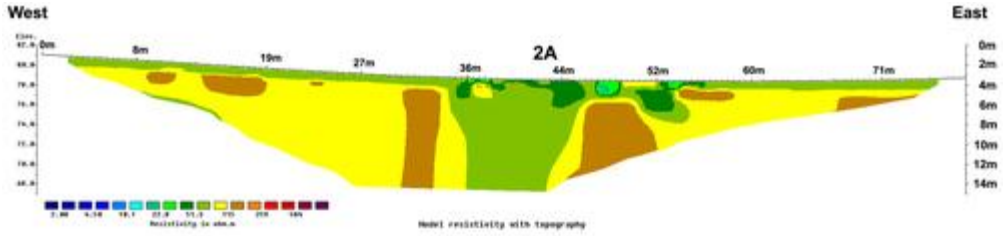

Figure 14: ERT profile (1m electrode spacing with topography) across 2A. Low-resistivity measurements coincide with the target. Colour legend: high resistivity (brown), low resistivity (blue)

At 5A plots were generated using an electrode spacing of both 1m (Fig. 15) and 2m (supplementary data file 4, fig. 4.11). The feature is indicated by an area of lower resistivity in comparison to the surrounding bedrock, and the results again demonstrate a similar pattern to those features interpreted as pits. Both sections imaged a slight layer of lower resistivity along the surface that corresponds to the relatively thin surface soil horizon, as is seen in pit 1A. The sides of the anomaly are gently sloping and indicate a feature with a diameter of approximately 20m. The base is indicated by a rapid increase in resistivity that is approximately parallel to the ground surface at a depth of 5m. Below the anomaly there is no disruption in the data that might suggest any further disturbance in the geology at depth.

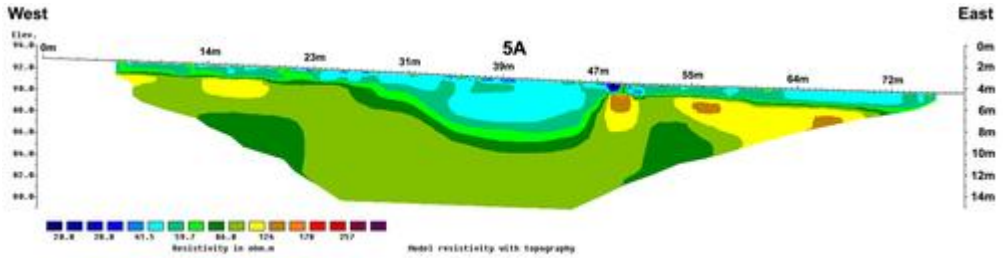

Figure 15: Results for ERT survey at anomaly 5A (top), 0.5m electrode spacing (bottom), 1m electrode spacing. Colour legend: high resistivity (dark red), low resistivity (dark blue)

The results for ERT survey over 7A, using an electrode spacing of 0.5m, are shown in Figure 16. The survey line was orientated in an east–west direction across the centre of the pit. Resistivity measurements ranged between 20 and 300ohmm, with the area of the pit marked by a decrease in near-surface resistivity compared to the surrounding area. The feature is approximately 20m wide, with sides that appear to slope gently.

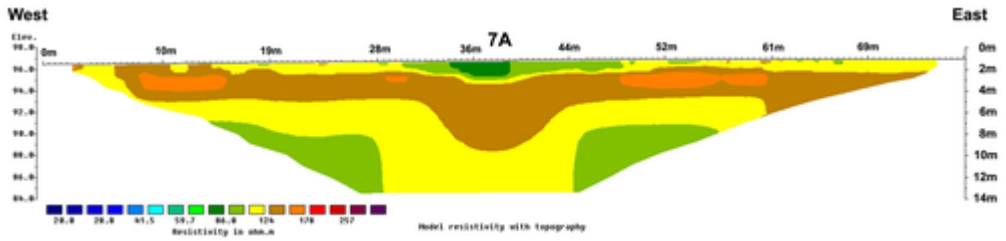

Figure 16: ERT profiles over 7A – (Top) 0.5m electrode spacing. Low-resistivity measurements coincide with the target feature. Colour legend: high resistivity (dark red), low resistivity (dark blue).

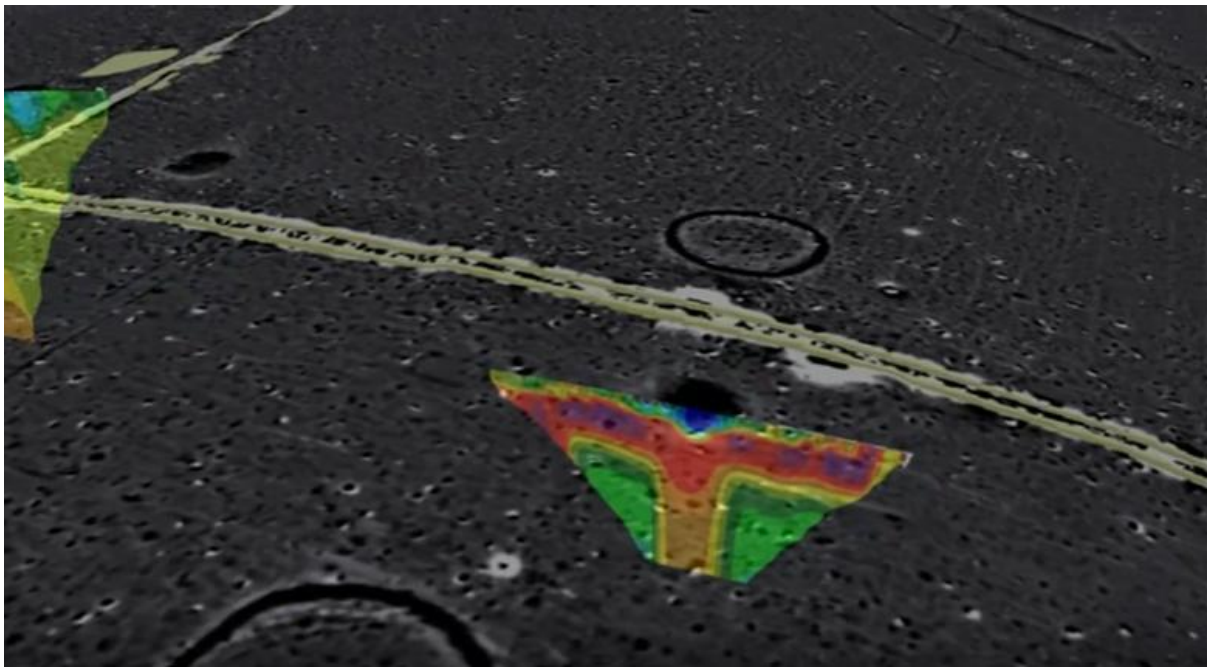

[ONLINE ONLY] (Bottom) Animation of ERT profile from 7A (0.5m electrode spacing) visualised in landscape setting with 2013 magnetometer survey overlay (courtesy LBI ArchPro, see Gaffney *et al*. 2020, supplementary data file 1). Colour legend: high resistivity (brown), low resistivity (blue). Greyscale legend: magnetometer – positive (black), negative (white).

A continuous ERT line (Figs 17–18) was acquired through features 2A, 3A, 4A and 5A, and utilised an electrode spacing of 3m. This was selected to assist in understanding the contrast in properties between the features and different superficial deposits. The line extended from west of 5A to east of 2A and, according to BGS mapping of the superficial geology, crossed from an area mapped with topsoil, but no superficial sediments, to an area that featured Head deposits consisting of clay, silts, sand and gravel. The 3m electrode spacing supported penetration to at least 20m with resistivity variation of between 20 and 300ohmm (supplementary data file 4, figs 4.7–4.10). Each of the target locations shows a consistent pattern of lower resistivity compared to the surrounding geology. The thin surface layer seen in the ERT surveys with closer electrode spacing was not imaged here. However, the character of the section is different in the near surface between 2A/5A and 3A/4A. It is suggested that 2A/5A are located at the edge or outside the Head deposits, whereas 3A/4A were within the Head deposits (Fig. 25). 2A and 5A provided the largest anomalous zones (low resistance/high conductivity), with cross-sectional distances of over 20m for each

anomaly, and a depth to base of approximately 5m. Features 2A/3A and 4A all show a small disruption in resistivity at depths greater than 5m that is wider than the anomaly zone itself. The contrast in resistivity here is smaller than the contrast within the anomaly zones and may be linked to the presence of Head deposits.

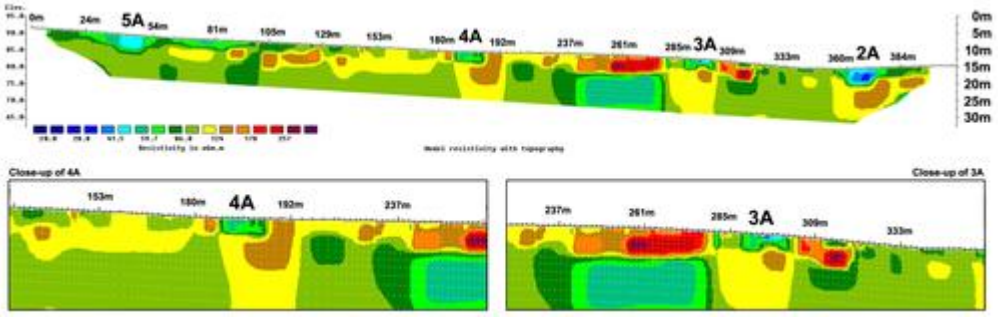

Figure 17: Long-line ERT profile (3m electrode spacing with topography) across 5A, 4A, 3A and 2A with close-up of 4A and 3A. Low-resistivity measurements coincide with the target features. Colour legend: high resistivity (dark red), low resistivity (dark blue)

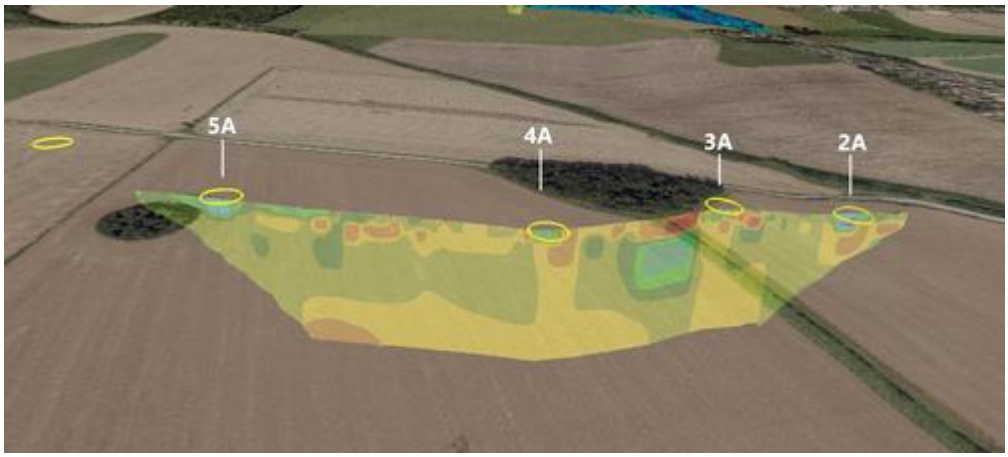

Figure 18: Landscape perspective – long-line ERT profile (3m electrode spacing with topography) across 5A, 4A, 3A and 2A. Low-resistivity measurements coincide with the target features. Colour legend: high resistivity (dark red), low resistivity (dark blue). Overlain on aerial photograph backdrop © Google Earth

5. Borehole Investigations

Features 1A, 2A, 3A, 13D and 16D were targeted for borehole investigation. Coring, as in 2019–20, was conducted mechanically with a Dando Terrier rig mounted on a small crawler unit. Core diameter size was a maximum 10cm or less. Opaque, black plastic liners were used to store the cores, and retention of a secondary core was considered for each surveyed feature, following an initial field assessment of the primary core. The opportunity was taken to recover a second core at 13D to increase the chances of finding dating evidence. Further methodological details of the borehole investigations are given in supplementary data file 6. Descriptions for cores taken from 5A and 8A in 2019 were published in Gaffney *et al*. (2020).

5.1 Core Analysis

The boreholes (summarised in Table 8, with imagery in supplementary data file 6) were successful in reaching the base of four of the target features. It was difficult to ascertain if the base of feature 2A was reached. This feature was cut into Pleistocene Head deposits rather than Chalk and defining the base of an infilled feature that is cut into sediments very similar to the fill units is difficult. Results of complementary ERT survey suggest this feature is less than 5m deep, which would suggest that the Pleistocene Head deposits are encountered where shattered flint cobbles were recorded in the core and at a depth of around 4.80m.

Core WS 1A consisted of a series of stratified clay-silt dominated units with variable flint content. Bedrock was reached at 4.65m depth. A possible buried soil was encountered between 2.70 and 2.88m depth. Core WS 2A was not bottomed onto Chalk, although the ERT suggested the base may have been at a depth of c.4.8m. The sediments in this core were typically finer grained than those in WS 1A. Core WS 3A consisted of an uppermost clay silt unit (top to 2m) overlying a flint gravel. Possible weathered Chalk was encountered at 6.9m depth. Core WS 16D consisted of stratified clay silts overlying probable Chalk bedrock at 5.75m depth. Core WS 13D (1) consisted of an upper red-brown clay silt to a depth of 2.8m, overlying pale yellow-brown clay silt to 4m. A further dark red brown, clay silt with flints lay above probable Chalk bedrock at a depth of 4.6m.

In most cases, the lithology of the sequences in the boreholes are consistent with feature fills. However, the thick gravel in WS 3A is unusual and potentially indicative of either deliberate filling of the feature or the presence of Pleistocene sediments beneath the feature.

Table 8: Summary of borehole investigations 2021

Core (window sample)	X	Y	Z	length (m)	topsoil (m)	natural (m)	Comment
WS 1A	415454	142717	82	6	0–0.3	4.65	bottomed
WS 2A	415003	142569	80	7	0–0.5	≥ 6.7m	-
WS 3A	414934	142565	83	7	0–0.5	6.90	bottomed
WS 13D (1) *first core*	414816	144762	92	5	0–0.6	4.60	bottomed
WS 13D (2) *second core*	414816	144761	92	5	0–0.3	4.65	bottomed
WS 16D	414907	144795	90	6	0–0.5	5.75	bottomed

5.2 Geochemical Analysis and Chemostratigraphy

Ninety-four samples were selected from three cores for analysis by inductively coupled plasma mass spectroscopy (ICP-MS) and inductively coupled plasma optical emission spectrometry (ICP-OES) techniques (see Table 9). Prior to analysis, all samples were dried and passed through a 2mm sieve to guarantee that large clasts of material were removed, ensuring that the finer grained matrix was analysed. The sieved material was ground to a fine powder in agate mortars. Following grinding, the samples were prepared for ICP analyses by using the lithium metaborate (alkali) fusion procedure, as advocated by Jarvis and Jarvis (1992a; 1992b). The prepared samples were then analysed using ICP-OES and ICP-MS instruments, with quantitative data being acquired for 49 major and trace elements. The precision and accuracy of the geochemical data acquired by the ICP analyses is determined by replicate analyses of multiple preparations of certified rock standard reference materials (SRMs), along with duplicate preparations of three unknown samples and are satisfactory for this study.

Table 9: Core window samples (WS) analysed by ICP techniques for this study. Cores were selected from both northern and southern 'arcs' based on sample availability and, where possible, overlap with other analyses

Core (window sample)	Samples analysed by ICP MS & ICP OES	Sample depth range (m)
WS 8A (2019-BH2)	38	0.50–4.93
WS 16D	37	0.96–5.85

WS 13D (1)	19	1.89–4.86

5.3 Chemostratigraphic Interpretation and Correlations

The results of the elemental analysis provided the foundation for constructing a chemical stratigraphy (chemostratigraphy) following the method described in Finlay *et al*. (2022). Initially, the data were evaluated statistically using Principal Component Analysis (PCA, Fig. 19). PCA is a statistical technique used to simplify multi-dimensional datasets while retaining the variation in the data. Therefore, as the ICP analysis produces data for 49 elements for every sample analysed in this study, the PCA establishes the main variations in the data. PCA analysis revealed three groups of elements, likely being driven by variations in the carbonate (chalk) and clay content, as well as elements probably associated with phosphatic material (possibly bone derived?), quartz or chert (possibly flint?) and detrital zircon variations (e.g. Finlay *et al*. 2022).

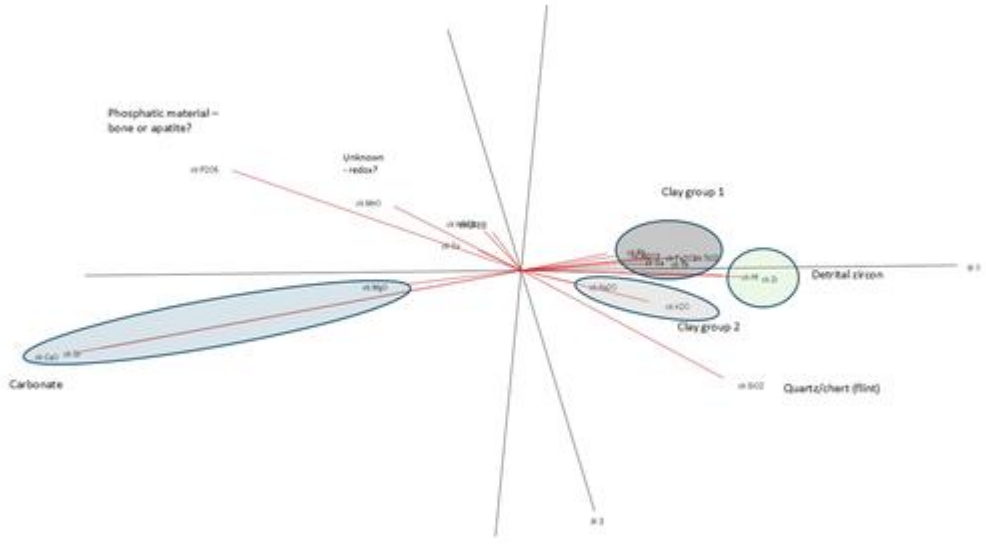

Figure 19: Principal Component Analysis (PCA) of all geochemical data collected in this study. Elements highlighted are labelled with probable control of composition, e.g. CaO and MgO likely reflect variations in carbonate (chalk) content of the analysed sample

After visual inspection of down-core variation, three elemental ratios were selected to establish four chemo zones (CZ1 –CZ4; Table 11) reflecting similarities in soil texture and mineral content.

- CaO/K_2O – likely reflecting variations in chalk and clay content
- Rb/K_2O – likely representing changes in clay mineralogy
- P_2O_5/K_2O – likely reflecting changes in phosphatic material (bone material?) and clay content

Chemostratigraphic correlation involves the characterisation, correlation or differentiation of sedimentary rock successions based on stratigraphic variations in the elemental geochemical data (see Finlay *et al*., 2022). As all three cores analysed in this study display the same elemental profiles, this enables these chemo zones to be chemostratigraphically correlated across several of the Durrington Walls pits (Fig. 20).

The boundary between chemo zones (CZ) 1 and 2 is well correlated across WS 8A, WS 13D (1) and WS 16D. It is defined by a downhole decrease in CaO/K_2O and increase in Rb/K_2O

and P_2O_5/K_2O. The boundary between CZ2 and CZ3 is well correlated across WS 8A, WS 13D (1) and WS 16D. It is defined by a downhole increase in CaO/K_2O and downhole decrease in Rb/K_2O and P_2O5/K_2O. The boundary between CZ3 and CZ4 is well correlated in cores WS 8A and WS 13D (1), but is poorly correlated into WS 16D, due to a sample gap. The CZ3 and CZ4 boundary is defined by a large downhole increase in CaO/K_2O and P_2O_5/K_2O values and a large decrease in Rb/K_2O values (Fig. 20 and Table 11).

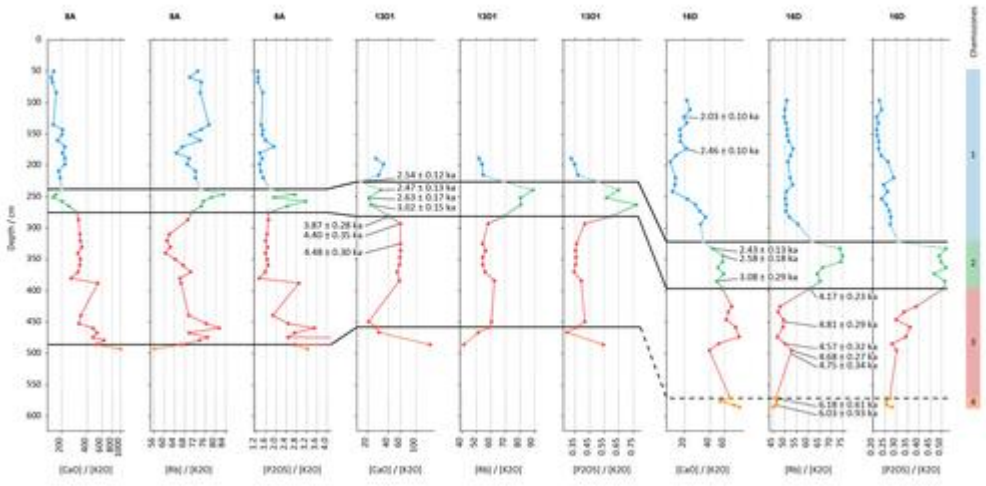

Figure 20: Chemostratigraphic correlation across core window samples (WS) from anomalies 8A, 13D (1) and 16D. The chemostratigraphy reveals three correlate zones based on changes in CaO/K2O (likely representing chalk/clay), Rb/K2O (likely representing changes in clay mineralogy) and P2O5/K2O (possibly bone content/clay minerals). Colour shading: blue = chemo zone 1, green = chemo zone 2, red = chemo zone 3 and orange = chemo zone 4

5.4 Optically Stimulated Luminescence (OSL) Dating

Optically stimulated luminescence profiling and dating (OSL-PD) was applied to the sediments recovered from cores WS 1A, WS 2A, WS 3A, WS 5A, WS 8A, WS 16D, WS 13D (1) and WS 13D (2) to determine dates for the construction of the pits and obtain chronologies for the sequence of infills (chemo zones 1 to 3). The methodological approach of OSL-PD as described in Kinnaird *et al.* (2025) was followed: in the first phase of the investigation, portable OSL equipment is used to appraise the luminescence properties of the sediment recovered from the core. Core WS 13D (2) was examined in the field immediately after recovery; however, cores WS 1A, WS 2A, WS 3A, WS 5A, WS 8A, WS 16D and WS 13D (1) were retrospectively examined in the laboratory. In the second stage, a representative sub-set of the samples are progressed to calibrated OSL screening and characterisation in the laboratory. Finally, after consideration of the stage 1 and 2 datasets, strategic samples from across the cores were progressed to quartz SAR OSL dating – stage 3. Further methodological detail for stages 1 to 3 is provided in supplementary data file 8.

5.4.1 OSL Results

A luminescence age is the quotient of the burial dose (measured in Gy) over the environmental dose rate (mGy a^{-1}). Table 10 lists the burial doses, total effective environmental dose rates and OSL depositional ages obtained from sediment recovered from cores WS 1A, WS 2A, WS 16D and WS 13D (1 and 2). The burial dose was determined through equivalent dose measurements on 24+ aliquots per sample using the single aliquot regenerative dose (SAR) OSL method (Murray and Wintle 2000). Figure 21

illustrates how the equivalent dose distributions vary with position in the core stratigraphy and in relation to the core chemostratigraphy. Environmental dose rates were calculated from the concentrations of K, U and Th determined by ICP-OES (K) and ICP-MS (U, Th) (as described above). The radionuclide concentrations were used to determine infinite matrix doses for α, γ and β radiation), using the conversion factors of Guérin *et al*. (2011), adjusted for attenuation by grain-size and chemical etching using the datasets of Guérin *et al*. (2012) and Mejdahl (1979), respectively.

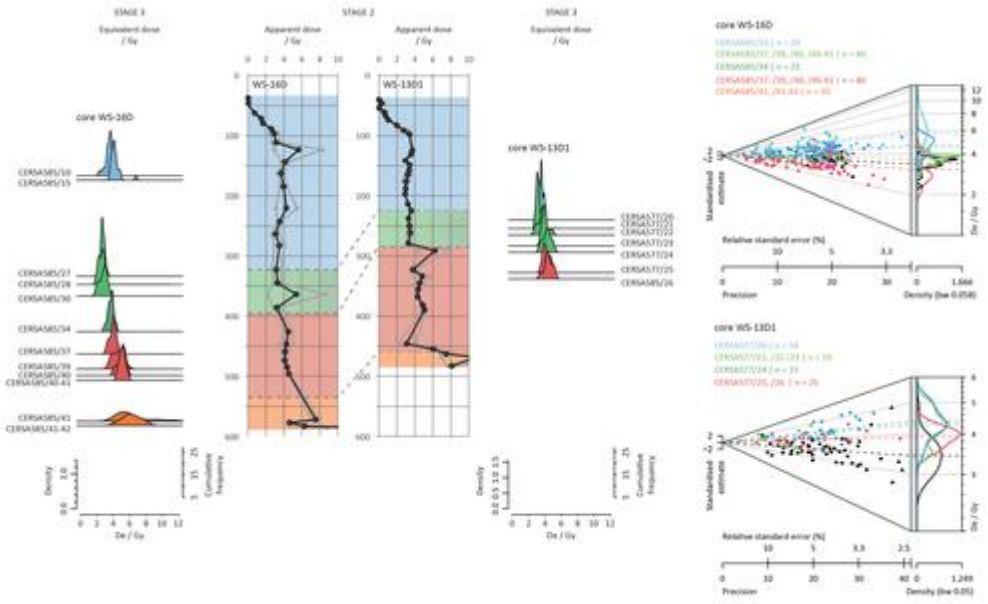

Figure 21: Equivalent dose distributions for samples from cores WS 16D and WS 13D (1), shown as kernel density estimate plots and Abanico plots. Colour shading: blue = chemo zone 1, green = chemo zone 2, red = chemo zone 3 and orange = chemo zone 4

Table 10: Results summary table of the burial doses, total effective environmental dose rates and OSL depositional ages obtained from sediment recovered from cores WS 1A, WS 2A, WS 16D, WS 13D (1) and WS 13D (2): core sub-samples are labelled with a sequential numeric suffix (see also supplementary data file 8 for further detail). Colour shading: blue = chemo zone 1, green = chemo zone 2, red = chemo zone 3 and orange = chemo zone 4

Field ID	Lab. code	Depth cm	Chemo zone	Palaeodose/Gy	Dose rate/mGy a^{-1}	Age/ka	Calendar years
WS1A-13	579-13	187	?	1.46 ± 0.04	1.04 ± 0.05	1.41 ± 0.08	AD 610 ± 80
WS1A-14	579-14	195	?	1.49 ± 0.05	1.00 ± 0.05	1.49 ± 0.08	AD 530 ± 80
WS1A-19	579-19	457	3	3.65 ± 0.15	0.71 ± 0.06	5.14 ± 0.48	3120 ± 480 BC
WS1A-20	579-20	464	3	2.68 ± 0.07	0.63 ± 0.06	4.24 ± 0.44	2220 ± 440 BC
WS1A-23	579-23	578	4	11.88 ± 1.73	0.69 ± 0.08	17.14 ± 3.14	>
WS1A-24	579-24	585	4	7.87 ± 1.67	0.71 ± 0.08	11.14 ± 2.67	>
WS1A-25	579-25	594	4	7.71 ± 2.40	0.72 ± 0.08	10.67 ± 3.53	>
WS2A-43	581/43	669	?	2.02 ± 0.05	5.19 ± 0.15	2.58 ± 0.1	550 ± 100 BC

WS2A-44	581/44	681	?	1.95 ± 0.08	4.38 ± 0.26	2.25 ± 0.16	220 ± 160 BC
WS16D-10	585-10*	123	1	3.27 ± 0.14	1.63 ± 0.05	1.94 ± 0.10	AD 80 ± 100
WS16D-15	585-15*	175	1	4.11 ± 0.10	1.69 ± 0.05	2.36 ± 0.10	340 ± 100 BC
WS16D-27	585-27*	333	2	2.67 ± 0.05	1.10 ± 0.05	2.36 ± 0.12	340 ± 120 BC
WS16D-28	585-28	344	2	2.53 ± 0.09	0.96 ± 0.05	2.64 ± 0.17	620 ± 170 BC
WS16D-30	585-30	385	2	2.52 ± 0.17	0.98 ± 0.06	2.55 ± 0.23	540 ± 230 BC
WS16D-34	585-34*	400	3	3.63 ± 0.08	0.89 ± 0.04	3.96 ± 0.21	1940 ± 210 BC
WS16D-37	585-37*	450	3	3.88 ± 0.09	0.82 ± 0.05	4.59 ± 0.28	2570 ± 280 BC
WS16D-39	585-39	484	3	4.49 ± 0.22	0.99 ± 0.05	4.53 ± 0.31	2510 ± 310 BC
WS16D-40	585-40	495	3	4.99 ± 0.20	1.08 ± 0.04	4.63 ± 0.26	2610 ± 260 BC
WS16D-40b	585-40 to 41*	500	3	5.07 ± 0.08	1.07 ± 0.07	4.62 ± 0.30	2600 ± 300 BC
WS16D-41	585-41	571	4	4.92 ± 0.41	0.81 ± 0.04	6.08 ± 0.60	4060 ± 600 BC
WS16D-41b	585-41 to 42*	582	4	4.59 ± 0.65	0.76 ± 0.04	5.87 ± 0.88	3850 ± 880 BC
WS13D1-19	577/19	215	1	3.27 ± 0.07	1.22 ± 0.07	2.69 ± 0.16	670 ± 160 BC
WS13D1-20	577/20	226	2	3.50 ± 0.07	1.38 ± 0.06	2.54 ± 0.12	520 ± 120 BC
WS13D1-21	577/21	239	2	3.05 ± 0.06	1.24 ± 0.06	2.47 ± 0.13	450 ± 130 BC
WS13D1-22	577/22	252	2	3.65 ± 0.16	1.39 ± 0.07	2.63 ± 0.17	610 ± 170 BC
WS13D1-23	577/23	263	2	3.90 ± 0.08	1.29 ± 0.06	3.02 ± 0.15	1010 ± 150 BC
WS13D1-24	577/24	281	3	4.18 ± 0.18	1.08 ± 0.06	3.87 ± 0.28	1850 ± 280 BC
WS13D1-25	577/25	293	3	4.04 ± 0.17	0.92 ± 0.06	4.40 ± 0.35	2390 ± 350 BC
WS13D1-26	577/26	325	3	4.38 ± 0.13	0.98 ± 0.06	4.48 ± 0.30	2460 ± 300 BC
WS13D2-9	587/9	443	2	4.49 ± 0.14	1.57 ± 0.06	2.87 ± 0.14	850 ± 140 BC
WS13D2-10	587/10	466	3	6.02 ± 0.20	1.32 ± 0.06	4.57 ± 0.25	2550 ± 250 BC
WS13D2-11	587/11	475	4	7.26 ± 0.67	1.22 ± 0.06	5.95 ± 0.62	3930 ± 620 BC
WS13D2-12	587/12	483	4	>	1.11 ± 0.07	>	>

Table 11 summarises the OSL and geochemistry of the cores (blue shading chemo zone 1, green chemo zone 2, red chemo zone 3 and orange chemo zone 4). It demonstrates coherent, comparable stratigraphies within each of the investigated cores. The base of CZ3 is dated to 2480 ± 130 BC, or 2350-2610 BC, based on the weighted combination of ages

across WS 1A, WS 13D (1), WS 13D (2) and WS 16D. This marks the pit base, so provides a constraint *terminus ante quem* for construction, i.e. mid-3rd millennium BC. There is little age-progression through the main body of CZ3, implying a rapid sedimentation rate. The transition from CZ3 to CZ2 is dated to between 1850 ± 280 BC and 1940 ± 210 BC (cores WS 13D (1) and WS 16D, respectively) and 1010 ± 150 BC and 850 ± 140 BC (cores WS 13D (1) and WS 13D (2)). The main body of CZ2 is dated to, most probably, between 610 ± 170 BC and 540 ± 230 BC, and the top, to 450 ± 130 BC and 340 ± 120 BC, cores WS 13D (1) and WS 16D, respectively. This implies that for the investigated cores, CZ2 was deposited over *c*.300–200 years. A single constraint for CZ1 was obtained in WS 16D, the sediment at 123cm depth in core returned an age of AD 80 ± 100

Table 11: Summary and interpretation of the chemostratigraphic analysis of core window samples (WS) from WS 8A, WS 13D (1) and WS 16D, with OSL ages for boundaries. Colour shading: blue = chemo zone 1, green = chemo zone 2, red = chemo zone 3 and orange = chemo zone 4

Chemo zone	OSL age	Depth (m) – core window sample			Interpretation
		WS 8A	WS 13D (1)	WS 16D	
CZ1	<340 BC				Organic-rich chalk-poor fill
Boundary	~540–340 BC	~2.38	~2.26	~3.22	
CZ2					Bone-rich unit with distinct clay mineralogy
Boundary	~1940–1850 BC	~2.75	~2.81	~3.96	
CZ3					Moderate chalk content increasing at base of zone, mirrored by clay content
Boundary	~2480 BC	~4.79	~4.58	~<5.71	
CZ4	~>4000 BC				Boundary with natural chalk basement

5.5 DNA Analysis

SedaDNA analysis was applied to 83 samples spanning cores WS 1A, WS 2A, WS 3A, WS 5A, WS 7A, WS 8A, WS 13D and WS 16D to determine the ecological composition of the cores, authenticate the presence of ancient DNA, and assess for evidence of taphonomic processes at work. Cores were sampled at the University of Warwick's ancient DNA facility under red light and subjected to CTAB-based DNA extraction (see supplementary data file 9 for methodology). Shotgun libraries (untargeted libraries of all DNA present) were prepared and sequenced on the Illumina NextSeq platform. After initial bioinformatic processing, taxonomic assignations were achieved using Phylogenetic Intersection Analysis (PIA) (Cribdon *et al*. 2020). SedaDNA reads were authenticated for damage using MetaDamage, which utilises the characteristic pattern of C-T and complementary G-A mismatches at the 5' ends of DNA molecules caused by cytosine deamination over time, typical of ancient DNA. Samples were assessed for evidence of post-depositional DNA movement through stratification and diffusion analyses, first described in Allaby *et al*. (2023). Stratification analysis tests whether DNA has moved after deposition by assessing whether read counts of taxa present in adjacent samples could have been drawn from the same underlying beta distributions. Diffusion analysis assesses the likelihood that DNA patterns are a result of diffusion between adjacent samples and estimates the proportion of the read counts observed that could be explained by diffusion from an adjacent sample. The analysis also employed a depositional model (Allaby *et al*. 2023) to estimate whether the DNA present originated from local sources (direct deposition) or originated from a distal source (associated with sediment source location) and brought in with influxing sediments.

Stratigraphic independence tests show that 82% of the taxa found within the pits sampled came from distinct underlying statistical distributions, indicating a generally stratified signal (see Table 9.1 in supplementary data file 9). This suggests that DNA is not undergoing

reworking/movement after it has been deposited. We also found little evidence of post-depositional DNA diffusion, supporting this conclusion (see Table 9.1 in supplementary data file 9). The depositional model showed that read counts were best explained by a mix of depositional scenarios. All sediments in this study were silts of varying colour; yellow, brown or red. When analysed as a combined group, regardless of colour, all sediments show that 57% of the DNA present is associated with sediments from influxing sources, while the remainder is attributable to an immediately local origin. When sediment types are considered separately, yellow silts show a dominant local signal, but the influence of distal sources is correlated with progressively darker sediments, with brown silts showing 93% of DNA is associated with distal sources and influxing sediments (see Table 9.2 in supplementary data file 9). These findings support the interpretation from the chemostratigraphy and OSL that the infilling of these pits may not have been due to natural processes since the sedaDNA taphonomy changes with the infilling process, suggesting a change from the original system and possible rapid periods of infilling in which the local signal becomes negligible. MetaDamage analysis shows a trend of increasing damage signature with increasing depth in the cores, supported by the OSL dates (Figs 9.1–9.8 in supplementary data file 9).

Our taxonomic assignations show that Durrington Walls likely resided in a meadow-like landscape, with a high proportion of large mammal signals (Ovis and Bos) present within the lower strata of the pits sampled. The deposition of these large mammal signals appears not to be random, with Ovis localised to the south and Bos present to the north and south (Fig. 22). The animal signals associated with ancient DNA correspond to chemostratigraphic zones CZ2 and CZ3 in cores WS 16D, WS 13D and WS 8A, which are bone/phosphoric rich zones, with bone fragments found at 4.79m in CZ3 of WS 8A.

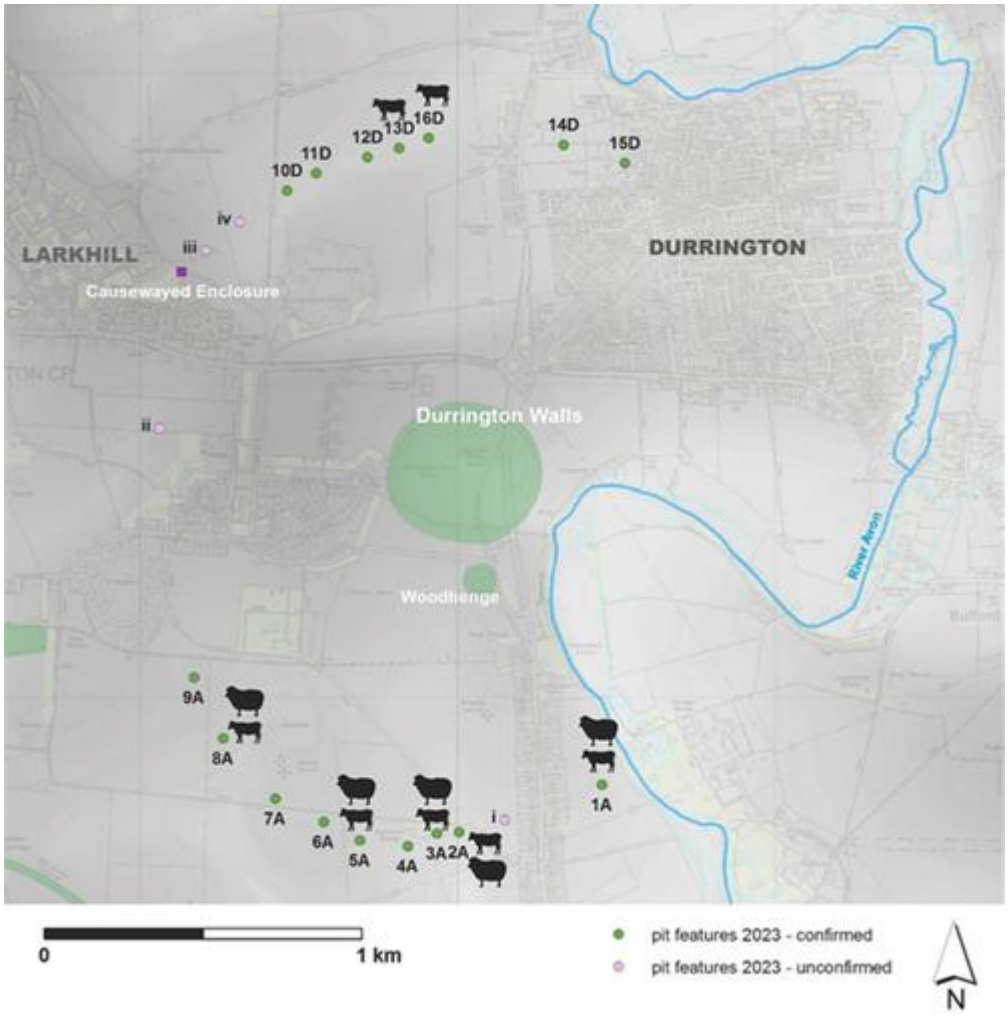

Figure 22: Location of the Durrington pits showing the distribution of Ovis and Bos signals within the pits sampled. Bos appear in all pits sampled, irrespective of location. Ovis appear to be localised to those pits to the south of the monument. Lidar-derived digital surface model (shaded) with OS 10K overlay © Environment Agency copyright and database right 2024. All rights reserved. Lidar (composite sources) DTM 1m resolution, Scale 1:4000 with gaps filled by DTM 2m resolution, Scale 1:8000 – Ordnance Survey (100025252)/EDINA supplied Service. http://digimap.edina.ac.uk

6. Comparison of Techniques Applied Across the Pit Alignment

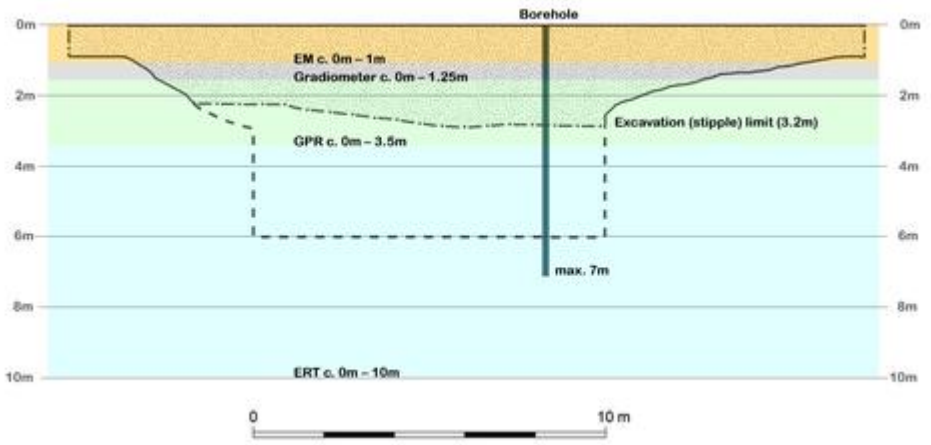

Figure 23: Schematic comparing depth penetration of investigative exploratory methods against potential pit depths and maximum depths of previous excavations undertaken prior to development

For illustrative purposes, Figure 23 provides a schematic overview of the relative depths of penetration of the various invasive and non-invasive techniques applied to the pit features near Durrington Walls Henge. To date, none of the recorded pits has been subject to total excavation. It is likely that the partial excavations that have been carried out were not able to clarify the nature of such large features. Mitigation excavations were of necessity limited and, in all likelihood, did not generally extend below the erosion cone of the features revealed by remote sensing. Coring, however, provided invaluable information on the sediments contained within each pit and underpinned the detailed analysis provided through geochemistry and sedaDNA as well as providing crucial dating evidence. Core data frequently confirmed the depth of individual features, although this was not the case in pits 2A, 5A or 15D (Table 1; Thompson and Powell 2018, 40–41). Moreover, individual cores could not provide information on the full geometry of these features. Consequently, information on the diameter and shape of specific pits was generally provided through remote sensing.

Unsurprisingly, individual remote sensing methods were unable to completely define the nature of these features. EM and gradiometry, as applied here, provided information on the shape of the upper levels of these features to a maximum of 1 to 1.25m, but did not generally penetrate beyond the weathering cone. In contrast, GPR could, under the best of conditions, penetrate beyond the erosion cone and up to 4m in depth. Time-slicing of the GPR data also provided information on the changing shape of the features beyond the erosion cone. This was key to confirming the uniformity of the surveyed pits both in size and shape, thereby linking them as part of a larger structure. Among the remote sensing techniques applied, only ERT located the base of pits consistently. However, the application of ERT at Durrington provided sections rather than plans and the spacing of the electrodes (0.5m, 1m, 2m, and 3m) necessarily reduced the resolution of the data in comparison to, for example, gradiometry.

Clearly, no individual technique provided the range of data required to characterise the Durrington Walls pit alignment. However, in the absence of a large and expensive excavation, the application of a range of techniques at Durrington has provided the information required to characterise the pit structure and certainly provides a model for the rapid exploration of similar massive features elsewhere.

7. Discussion

As stated in the introduction, the original intent of this article was to provide supplementary information to that contained within our earlier publication on the pit group surrounding Durrington Walls (Gaffney *et al*. 2020). However, the emphasis here was necessarily modified to consider published discussion of the earlier work, and notably that contained in articles by Ruggles and Chadburn (2024) and Leivers (2021). While the authors are aware that the history of research in the Stonehenge landscape is littered with contentious claim and counter claim, not all of which are of equal value, the team felt that, on this occasion, a response was required.

The arguments provided by Ruggles and Chadburn (2024) essentially highlight several key issues. It is asserted that the original publication demonstrates the dangers of data selection, as well as of biased interpretation, 'not least because many of the areas in and around the “circle” have not been investigated. Many comparable features being omitted' (Ruggles and Chadburn 2024, 104). The dating of the investigated features was also considered suspect, with individual pits varying in date by around 4000 years. Following these observations, it is claimed that the pit circle identified in our earlier paper is a portmanteau, comprising a series of unrelated and unverified features, some of which had been identified as sinkholes

Although survey has demonstrated that those features interpreted as pits are similar in character, size and depth, and that these observations are replicated north and south of Durrington Walls (Fig. 1), Ruggles and Chadburn suggest that the separation of these features as a distinct and coherent group is a result of biased decision-making. To demonstrate this, their article includes a map of known archaeological features in the vicinity of the southern arc of features (Ruggles and Chadburn 2024, fig. 3). The absence of any consideration of these sites within the original paper is held to be evidence for selective interpretation. In fact, the entire area of Durrington Walls and the adjacent land has been surveyed by the Stonehenge Hidden Landscapes project. Although subject to a separate publication process, some of the information for these features has already been released and utilised by other academics (Gaffney *et al*. 2018, figs 1 and 2; Bowden *et al*. 2015, table 3.1). However, for the purposes of this article, the relevant data are reproduced in Figure 24. Setting aside the three pit features (4A, 6A and 9A). which are clearly not transcribed by Ruggles and Chadburn in their correct position, consideration of the geophysical anomalies associated with the remaining 'comparable' features confirms that these cannot be analogous with those selected for study as part of this sub-project. Most archaeologists would readily interpret these as Neolithic mortuary structures, simple and complex ring features and later enclosures, and morphologically distinct from those studied as part of this and the 2020 paper (see supplementary data file 10 for detail on individual sites).

Figure 24: Top – features recorded as potential comparator data for those features identified as pits (after Ruggles and Chadburn 2024, fig. 3). Bottom – magnetic anomalies (1A–9A) and potential anomaly i overlain OS 10K mapping. Fluxgate gradiometer survey mapped as part of the Stonehenge Hidden Landscapes Project and supplied by LBI ArchPro, Vienna. Note the clear qualitative difference between features identified as potential pits and those suggested as comparators (see supplementary data file 10 for detail). (Top) OS 10k overlay with aerial base map 25cm (Get Mapping) – Ordnance Survey (100025252)/EDINA supplied Service; Department of Environment, Food & Rural Affairs (Defra), 'Scheduled Monuments' [last accessed: 18.09.2024] (Bottom) OS 10K underlay © Crown and database rights 2024. All rights reserved. – Ordnance Survey (100025252)/EDINA supplied Service. http://digimap.edina.ac.uk

Consequently, far from being impacted by 'Missing Data', as Ruggles and Chadburn's original paper suggested, the results presented here are part of a larger dataset that clearly distinguishes these features from any others adjacent to Durrington Walls. The exclusion of any monument in our previous publication was primarily the result of an interpretation based on their geophysical response. That, along with information recorded in publicly available archives, demonstrated that excluded features were not comparable with those anomalies selected for detailed study and which appeared to form part of a coherent cluster (https://historicengland.org.uk/listing/the-list/).

Having asserted the consistency of the features in morphological terms, a comment on the potential origin of the features forming the Durrington pit alignment is required. Ruggles and Chadburn (2024) and Leivers (2021) suggest that a significant number of pit-like features, notably in the north, are of natural origin and probably sinkholes, and that the putative pit

structure should be discounted on that basis. While they do not actually provide any justification for this statement, it should be noted that our original paper (Gaffney *et al*. 2020) did not discount the origins of some of these features as natural. Indeed, it was stressed that '*if any of the features near Durrington originate as natural features, it seems reasonable to suggest that a larger monumental circle may have emerged, centred on the area of the Durrington Henge, and involving tens of similar, massive pits*' (Gaffney *et al*. 2020). Given the lack of a comprehensive excavation of any of these features it is better that we turn to the wider geological context for explanation.

Geologically, all the features under investigation here are located on a layer of Late Cretaceous Chalk which is approximately 85 million years old. These rocks are locally called the Seaford Chalk Formation. Features 2A, 12D and 13D lie within dry valleys with superficial head (clay, silt, sand and gravel) deposits, while features 3A, 4A and 5A are associated with superficial head (gravel) deposits (Figure 25).

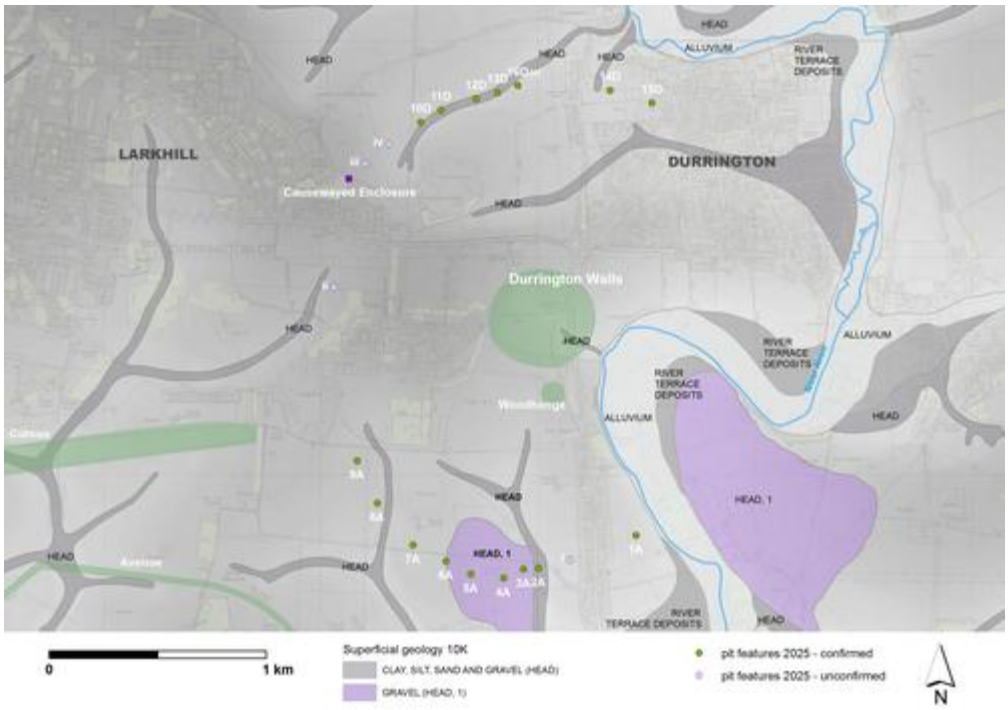

Figure 25: Geological overview of probable and possible pits in relation to superficial head deposits of clay, silt, sand and gravel often associated with dry valleys (marked in grey). As regards pits investigated in 2021: 3A, 4A, and 5A occur within area of Head deposit, 1 - gravel (BSG REF 625), while 2A and 13D occur within areas of Head deposit - clay, silt, sand and gravel (BSG REF 424). © Crown copyright and database rights 2024 – Ordnance Survey (100025252)/EDINA supplied Service (OS MasterMap® Scale 1:1250 and OS Profile DTM (5m resolution) Scale 1:10K); British Geological Survey/EDINA supplied service (BGS Superficial deposits 1:10K – Sheet SU14SW v2.18). http://digimap.edina.ac.uk

Several characteristics associated with active sinkholes can be considered when examining the likely origin of our features. According to Waltham *et al*. (2005), active sinkholes in the United Kingdom are often small and of limited distribution. However, buried sinkholes are common near the chalk and Tertiary bedrock contact (Waltham *et al*. 2005) and their formation process often necessitates the presence of overlying Tertiary sediments. Today there is no Tertiary sediment cover in the vicinity of the study area. Sperling *et al*. (1977), who examined the density of solution hollows on the chalk in Dorset, note their high density, reaching 99/km^2 at Southover Heath and 157/km^2 on Puddletown Heath but without any

discernible patterns of distribution. The size of the features in the Dorset study has the modal distribution between 10–20m while their average depth (rampart to centre) is typically 2–4m. Mapping of the distribution of sinkholes within the Salisbury Plain area (Hopson *et al*. 2006) clearly shows that sinkholes throughout the district are associated with the river drainage networks across the region rather than being distributed across the flatter interfluves between the rivers, as is the case for a significant number of the features forming the Durrington pit circle.

Structurally, natural solution features in chalk exhibit a thin, blackish clayey band, usually up to 1cm in thickness between the chalk bedrock and the sediments infilling a solution feature (Chartres and Whalley 1975). The contact with the underlying chalk rubble is always sharp but the contact into the overlying loamy gravels is often graded over 10–50mm. This black band of clay is often continuous around the whole margin of the solution feature but is notably absent in those features cored to bedrock as part of this study (Fig. 26).

The origin of sinkholes remains somewhat opaque. Sperling *et al*. (1977) suggest that, in Dorset, these features result from intense and localised solutional activity promoted by highly acidic conditions under heathland conditions. The association of the distribution of Tertiary sediments with solution in the underlying chalk is indicative of the activity of underground processes at work in the creation of the sinkholes rather than necessarily formation occurring under subaerial conditions (Jeffrey *et al*. 2020). Thorez *et al*. (1971) have demonstrated that around South Mimms the fills of solution features are predominantly derived from the Tertiary sediments, indicating formation beneath the Tertiary cover rather than subaerially.

Figure 26: Top Left – Station Quarter South Ebbsfleet solution features. Note the dark brown contact between the Chalk and overlying sediments. Top Right – Large pit cut through chalk and Thanet Sand near Ebbsfleet, Kent. Note steep sides, sub-horizontal bedding and lack of the brown rim along the edge one finds in solution hollows. Bottom – Solution features in the Chalk at Dartford A2/M25 works. Note the undulating surfaces and the haphazardly filled features

Consequently, we argue that these features are not sinkholes as they do not conform to the internal structure, or distribution, commonly associated with such features. Furthermore, such features are typically of some antiquity (e.g. in Kent, Middle and Lower Palaeolithic material can be found in such features) and consequently the young age of the fills dated as

part of this project mitigates against a natural origin. Most significantly, perhaps, is the observation that the formation processes necessary to create such natural features cannot have existed within the time frames indicated by the dating of the sediments infilling the features reported here. If creation of natural sinkholes requires a cover of Tertiary sediments over the chalk, then such a cover would have to have existed prior to and during the Neolithic period, as indicated by the dating evidence from the features. Subsequently this cover would have to be removed across the whole of the study area. There is no indication of such large-scale stripping of Tertiary sediments in this landscape currently. A final point relates to the geometry of the structure. The initial publication recorded the location of large pit-like anomalies, derived from remote sensing and other available data, across the Stonehenge landscape (Gaffney *et al*. 2020, fig. 9, see also supplementary data file 10, section 10.3, figure 10.6). The proposed structure is clearly distinct from other recorded features, primarily in the manner in which the pits appear to conform to a band *c*.864m from the boundary of the henge (Gaffney *et al*. 2020, figs 22 and 23). This distinctive pattern emerges irrespective of topography and presents an arrangement that most would regard as unusual if these were solely composed of natural features.

If the features, overall, are unlikely to be of geological origin, what then can we determine from the evidence provided through the chemostratigraphic and dating programmes applied to the cores retrieved from individual pits? It is certainly not possible to confidently distinguish whether fills are formed by natural infilling or by anthropogenic processes from chemistry alone. The chemostratigraphy, combined with OSL dating, demonstrate that the fills within the studied pits comprise three chemically and chronologically distinct units that correlate across the site (Fig. 20). This regularity of pit fills around Durrington Walls could be explained by a 'layer cake' stratigraphy across the entirety of the superficial geomorphology of the general Durrington area. However, the geophysics show that these features are distinct within the landscape. Furthermore, Core 13D (1) is sited inside a different superficial geological unit to core 16D (Fig. 25) and therefore it is highly unlikely if both features were natural that they would have the same fill composition. The chemostratigraphy (along with the lithology) also suggests that the boundaries between these units are sharp. Such patterns conform to those seen in cut features and in contrast with rather more gradational contacts seen in natural solution hollows (see Fig. 26).

Ruggles and Chadburn (2024) assert that the dating of the investigated pits is suspect, with features varying in date by around 4000 years. In fact, detailed OSL dating undertaken during this study shows that the chemostratigraphic boundaries in cores WS 1A, WS 13D (1), WS 13D (2) and WS 16D are of equivalent age, within error, providing a constraint for the base of CZ3 at 2480 ± 130 BC, or 2350-2610 BC, which also provides a *terminus ante quem* for construction of these pits (Table 10 and Table 11). The top of CZ3 is dated to *c*.1900 ± 170 BC, and there is likely a hiatus between deposition of CZ3 and CZ2, with CZ2 dated to between 610 ± 170 BC and 340 ± 120 BC in cores WS 13D (1) and WS 16D. Ruggles and Chadburn (2024) highlighted the inversion observed in the radiocarbon ages reported in Gaffney *et al*. (2020) for core WS 8A. Gaffney *et al*. (2020) argue for construction of pit 8A in the mid 3rd millennium BC, based on the basal radiocarbon date of 2460-2270 cal BC (78%) or 2260-2200 cal BC (17%). This is in good agreement with the dates for construction of pits 1A, 16D and 13D. The additional dates in core WS 8A – 3930-3870 cal BC (11%) and 3810-3690 cal BC (84%) at 435-440cm depth and 4750-4550 cal BC at 150-155cm depth are from parts of the cores that were shown to be re-deposited. In these parts of the sequences, the sediment is characterised by intensities in excess of the down-profile signal-depth progression, i.e. the luminescence is dominated by residual signals. These instead provide an insight on the adjacent landscape and palaeo-environment, and a *terminus post quem* for sediment in the immediate vicinity to the pits (a conclusion corroborated with the OSL ages obtained for CZ4, >*c*.3850 BC). Gaffney *et al*. (2020) also argued for recuts within the pits, based on a radiocarbon date of 1390–1340 cal BC (13%) or

1310–1160 cal BC (79%) or 1150–1130 cal BC (3%) from 5.18m depth in WS 5A. This agrees with the OSL ages obtained at the transition between CZ3 and CZ2 in WS 13D (1) and WS 13D (2). Consequently, rather than being a recut, this probably indicates the same chemostratigraphy in WS 8A as WS 1A, WS 13D (1), WS 13D (2) and WS 16D. Thus, the independent chronologies are in agreement and, together with the geochemistry and sedaDNA damage proxies, suggest that it is highly unlikely that the consistent fills across the larger area of the site are natural. Instead, it is more likely that some of these pits may have been deliberately filled in a similar manner, or process, during parts of their histories.

8. Conclusion

The results of fieldwork presented here supports previous assertions that Durrington Walls henge is surrounded by a ring of massive pits that form a cohesive structure incorporating the earlier Larkhill Causewayed Enclosure (Gaffney *et al*. 2020). Contra Ruggles and Chadburn (2024), those features that they highlight as missing from our interpretation differ significantly to those identified as pits (see supplementary data file 10). As was stressed in our earlier publication, some pits may well have originated as natural features. However, since none of the features identified through fieldwork have been fully excavated, there is currently no evidence to support such an assertion, in the manner attempted by either Ruggles and Chadburn (2024) or Leivers (2021). Despite this, it remains true that, while the consistent size, shape and depths of those features interpreted as pits suggest linkage, it is not possible to definitively exclude the existence of other, perhaps earlier, structures within such large features.

Setting aside the significance of internal features that are currently hypothetical, it remains true that not all the cored features provided a detailed chronology. However, fieldwork has produced temporal evidence for complete stratigraphic profiles of individual pits, and the results of OSL dating, combined with the geo-stratigraphic and DNA analysis presented here, suggest that pits across the cluster are characterised by consistent morphological profiles. They also support a later Neolithic date for the emergence of the pit alignment. There is, furthermore, the possibility that some of these features, at least, may have been deliberately infilled, and that the DNA data provides intriguing evidence for structured deposition or, at least, the preferential presence of animals between the northern and southern arcs of pits, and perhaps a distinction between upper and lower pit deposits. Such a statement is necessarily provisional, although the evidence for structured deposition of animal parts at Woodhenge provides a context for such observations (Pollard 1995). Published data from pits in the Stonehenge region also hints at changes in meat preferences across the Neolithic (Worley *et al*. 2019). Consequently, given the stratigraphic position of the sedaDNA samples, there is a possibility that such patterns may have a temporal aspect. The value of further work to establish the role of sedaDNA analysis within terrestrial, archaeological field work is evident from the study presented here, but the cumulative evidence for the cultural context of such detail is gradually emerging.

Having demonstrated the likely cultural component of the pits, is it possible to add to the interpretation presented as part of the original paper? That publication contained a summary of the evidence for the digging of substantial pits elsewhere during the Neolithic. While it is not the intention to repeat such information, our knowledge of such activities has progressed since the work at Durrington Walls was initiated. It is noteworthy that the practice of digging very large pits during the Mesolithic period is attracting increasing archaeological interest across Britain (Gaffney *et al*. 2013; Luke and Kozimiński 2023; Wolframm-Murray 2024). Examples of recent finds include the cluster of large pits at Milltimber, Aberdeenshire (Dingwall 2018), while the recent discovery of at least 25 large pits at Linmere, in Bedfordshire, adds significantly to the corpus of such finds. Excavated by Museum of London Archaeology (MOLA) and Albion Archaeology, these features are asserted to be of a

monumental scale, and up to 5m wide and 1.85m deep (Gaffney *et al*. 2023). Dated between 8500 and 7700 years ago, the excavators state that the current pit count is unlikely to represent the total number of such features. The pits do not appear to have a hunting or storage function, while their location next to water and, potentially, their arrangement suggest a 'special significance' (Alberge 2023). The presence of individual large, Mesolithic pits, including examples at Stonehenge, also indicate the archaeological value of such apparently prosaic features (De Smedt *et al*. 2022). There is therefore an increasing context for the special nature of large pits, individually or in clusters, dating from the Mesolithic at least, while the evidence from later periods incorporates formal monuments that may include, or be composed of, pit-like features (Gaffney *et al*. 2020).

While the size and scale of the pit circle at Durrington might, initially, be considered surprising, the alignment is set within a landscape that is testament to the capacity of prehistoric communities to invest in the construction of large, and frequently unique, monuments. The construction of a pit circle, even at the scale demonstrated at Durrington, was clearly not an exceptional act for communities that could erect Stonehenge. Consequently, as data accumulates on the extended history and significance of pit-digging in prehistory, the lesson may be that the existence of large pit clusters or structures should probably be anticipated during fieldwork, rather than simply encountered. We should certainly not dismiss such features as natural, coincidental or insignificant to past communities.

There are, nevertheless, characteristics of the Durrington pit group, and its development, that do deserve further comment, even when set within a landscape as complex as that surrounding Stonehenge. The significance of emergent complexity within archaeological landscapes is well established (Tilley 1994), and the potential for monument groups to be ordered at a very large scale has been demonstrated elsewhere. Examples include New Grange (Condit and Keegan 2018 2020; Davis and Rassmann 2021), and such patterning has been claimed, recently, in the distribution of stone circles on Dartmoor (Morris 2024). Stonehenge, unsurprisingly, has seen repeated attempts to interpret the cosmology behind the spatial structures of the monument and its surrounding landscape (Darvill 1997; Parker Pearson and Ramisillona 1998). How we perceive order within complex monumental landscapes is therefore of considerable significance when assessing phenomena like the Durrington pits. When considering such issues, Bradley's (1998) discussion of the role of time in the creation of monuments and their landscapes is particularly instructive. He notes that the contemporary concept of time frequently inhibits interpretation of complex, ritual structures (1998, 87). Bradley emphasised the role of social time, and the long repetition of liturgical actions, in ordering both the landscape and society, and noted that such order is frequently situated in reference to the past. When published, Bradley cited Woodward and Woodward's (1996) paper on the configuration of burial mounds around Stonehenge as an example of such a process. It had been suggested that these mounds formed two concentric circuits and reflected, in some manner, the monument itself. The significance of circular arrangements and structures in prehistory is, of course, well documented and has attracted substantive commentary (Bradley 2012, see also supplementary data file 10). In retrospect, however, such interpretations are only partially correct for the Stonehenge landscape. Later study of the burial mounds surrounding the Stonehenge indicated that the apparent placement of mounds may have been the result of many different, largely visual, links to a number of earlier monuments (Exon *et al*. 2001). What remains true, as Bradley has noted, is that in the Stonehenge landscape, 'like the Renaissance Theatre of Memory…, every element referred to something in the past' (1998, 100). The implication of such an observation is that the spatial order that archaeologists observe within a monument group may not be inherent, but achieved without direct intentionality over significant time scales. In the case of Stonehenge, it could never have been the intention of those who initially established the monument that it would be surrounded by tumuli. Yet, the presence of

Stonehenge, and its topographic setting, was clearly essential to the siting of later burial mounds. The resultant, perceived order, usually interpreted by archaeologists as a monument complex, was not in itself a mere reflection of the belief structures of individual communities separated by millennia, but is better understood as a development contingent upon earlier, and frequently unrelated, decisions.

Evidence for emergent patterning is recorded elsewhere in the natural world and is often interpreted as evidence for *stigmergy*: a term coined by zoologist Pierre-Paul Grassé (1959). This originally referred to the effect of pre-existing environmental states on the actions of termites when constructing mounds. These have apparent form and function but arise without any requirement for planning or direct communication. It seems likely that stigmergy also occurs in other social species, including humans (Ch'ng *et al*. 2014; Helbing *et al*. 1997a; 1997b). The manner in which large monumental structures emerge over time, and display apparent order, may therefore be examples of such a process, and the pits at Durrington could be interpreted in a similar manner. This does not, of course, suggest that the resultant order was not culturally significant or uninterpretable. The Durrington pit cluster, for example, appears to relate directly to the existence of the henge monument at its centre, yet also incorporates the earlier causewayed enclosure at Larkhill within the circuit. The cosmological significance of appropriating past monuments in this manner would certainly have been meaningful to contemporary societies and the social structures that underpinned such built landscapes.

However, while the ordering of, for instance, the tumuli around the Stonehenge visual envelope arises from the specific situation of Stonehenge and the natural variation of the surrounding topography, this is not necessarily the case for the Durrington pits. As stated in the original paper, there is no consistent visual relationship between the pit group and the henge monument that it surrounds. If there is a definable relationship between these features, it seems to lie in the deliberate positioning of the pits to reflect the distance between the henge and the earlier Larkhill causewayed enclosure. Our earlier publication suggested that the configuration of pits and monuments indicated the use of a numeric system, and that the imperfect nature of the circuit probably derived from the use of pacing to set out the ring. In contrast to many situations in prehistory in which intervisibility and topography act as primary drivers, the Durrington pits demonstrate a different level of intentionality. This is indicated by the evidence for mensuration and, through that act, a very different mode of control over the landscape. Ultimately, this, and the landscape scale at which the circuit of pits has been created, remains unusual and currently unique for this period, within Britain at least.

Such a statement remains, of course, an interim position without further detailed study and probably, the total excavation of one or more of the features forming the larger pit circle. Despite that requirement, the results presented here, from a second season of fieldwork at Durrington Walls, demonstrate that the published critique presented by Ruggles and Chadburn (2024), is not upheld. The weight of evidence continues to indicate that 'a series of features, most likely large pits, surrounds the Durrington Walls henge enclosure', and that 'this group represents an elaboration of the monument complex at a massive, and unexpected, scale' (Gaffney *et al*. 2020). Moreover, the improved dating evidence suggests that, irrespective of the histories of individual pits, the larger group likely emerges as a cohesive structure during the Late Neolithic.

Acknowledgements

A full list of individuals and contractors involved in fieldwork supporting this article is contained in supplementary data file 11. Here we would like to acknowledge and thank the National Trust, and Dr Nicola Snashall, for facilitating the fieldwork reported here, as well as

tenant farmers Bill King and Hugh Morrison for providing access to undertake the fieldwork on National Trust land. The Ministry of Defence and Dr Richard Osgood also supported the fieldwork reported here, along with tenant farmers Ian Baxter and Mathew Reed, who provided access for fieldwork on MoD land. Further thanks to landowners Bill King and Hugh Morrison for permitting access to privately owned farmland. We were very pleased to work with Wild Blue Media, and particularly Cameron Balbirnie, Kate Dooley and Rachel Vaknin, both during fieldwork, on the accompanying documentary and while preparing this article for publication. We must express our thanks to Professor Richard Bradley who provided advice during the preparation of this report.

The original magnetic survey of the southern pit group was undertaken as part of the 'Stonehenge Hidden Landscapes Project': an international, collaborative research programme supported through the Ludwig Boltzmann Institute for Archaeological Prospection and Virtual Archaeology (https://archpro.lbg.ac.at) incorporating the Ludwig Boltzmann Gesellschaft (Austria), Amt der Niederösterreichischen Landesregierung (Austria), the University of Vienna (Austria), the Vienna University of Technology (Austria), ZAMG Central Institute for Meteorology and Geodynamics (Austria), Airborne Technologies (Austria), 7reasons (Austria), ÖAW– Austrian Academy of Sciences (Austria), ÖAI – Austrian Archaeological Institute (Austria), RGZM Mainz – Römisch-Germanisches Zentralmuseum Mainz (Germany), the University of Birmingham in collaboration with the University of Bradford (GB), Arkeologerna of Statens Historiska Museer (Sweden), NIKU – Norwegian Institute for Cultural Heritage (Norway), and Vestfold fylkeskommune – Kulturarv (Norway).

The authors would like to thank the anonymous reviewers of the article for their consideration and thoughtful comments on the original text.

Supplemental Data → [ONLINE ONLY]

Bibliography

AAME 2023 'The Aerial Archaeology Mapping Explorer (AAME) portal', *Historic England* [website] https://historicengland.org.uk/research/results/aerial-archaeology-mapping-explorer/ [Last accessed: 28 May 2025]

Alberge, D. 2023 'Discovery of up to 25 Mesolithic pits in Bedfordshire astounds archaeologists', *The Guardian* [website], 3 June 2023. https://www.theguardian.com/science/2023/jul/03/discovery-25-mesolithic-pits-bedfordshire-astounds-archaeologists [Last accessed: 26 March 2025]

Allaby, R., Ware, R., Cribdon, R., Hansford, T., Kinnaird, T., Hamilton, W., Kistler, L., Murgatroyd, P., Bates, R., Fitch, S. and Gaffney, V. 2023 'Pleistocene-Holocene sedaDNA reconstruction of Southern Doggerland reveals early colonization before inundation consistent with northern refugia', 21 September 2023, PREPRINT (Version 1), *Research Square*. [Last accessed: 11 June 2025] https://doi.org/10.21203/RS.3.RS-3296992/V1

Baldwin, E. and V. Gaffney 2020 'Interim report on the recent discovery of a series of massive pits near the Durrington Walls henge', Unpublished Report for the National Trust, University of Birmingham

Bøtter-Jensen, L., McKeever, S.W. and Wintle, A.G. 2003 *Optically Stimulated Luminescence Dosimetry*, Amsterdam: Elsevier. https://doi.org/10.1016/B978-0-444-50684-9.X5077-6

Bowden, M., Soutar, S., Field, D. and Barber, M. 2015 *The Stonehenge Landscape. Analysing the Stonehenge World Heritage Site*, Swindon: Historic England.

Bradley, R. 1998 *The Significance of Monuments*, London: Routledge.

Bradley, R. 2012 *The Idea of Order: The Circular Archetype in Prehistoric Europe*, Oxford University Press. https://doi.org/10.1093/oso/9780199608096.001.0001

Ch'ng, E., Gaffney, V. and Hakvoort, G. 2014 'Stigmergy in comparative settlement choice and palaeoenvironment simulation', *Complexity* **21**(3), 59–73. https://doi.org/10.1002/cplx.21616

Chartres, C.J. and Whalley, W.B. 1975 'Evidence for Late Quaternary solution of Chalk at Basingstoke, Hampshire', *Proceedings of the Geologists' Association* **86**(3), 365–72. https://doi.org/10.1016/S0016-7878(75)80027-7

Condit, T. and Keegan, M. 2018 'Aerial investigation and mapping of the Newgrange landscape, Brú na Bóinne, Co. Meath. The Archaeology of the Brú na Bóinne World Heritage Site Interim Report, December 2018, Department of Culture, Heritage and the Gaeltacht', *Voices from the Dawn* [website]. https://voicesfromthedawn.com/wp-content/sites/newgrange/bru-na-boinne-interim-report_web.pdf [Last accessed: 11 June 2025]

Condit, T. and Keegan, M. 2020. 'A Neolithic ritual landscape revealed: A summary of the principal sites that were identified on the Newgrange floodplain during the drought conditions of summer 2018', *OPW – Oidhreacht Éireann/Heritage Ireland* [website] https://heritageireland.ie/articles/a-neolithic-ritual-landscape-revealed/ [Last accessed: 11 June 2025]

Cribdon, B., Ware, R., Smith, O., Gaffney, V. and Allaby, R. 2020 'PIA: more accurate taxonomic assignment of Metagenomic Data demonstrated on sedaDNA from the North Sea', *Frontiers in Ecology and Evolution* **8**(84). https://doi.org/10.3389/fevo.2020.00084

Crutchley, S. 2002 'Stonehenge World Heritage Site Mapping Project: Management Report', Aerial Survey Report Series AER/14/2002, Swindon: English Heritage. https://historicengland.org.uk/research/results/reports/6835/StonehengeWorldHeritageSiteMappingProject_ManagementReport [Last accessed: 28 May 2025]

Darvill, T. 1997 'Ever increasing circles: the sacred geographies of Stonehenge and its landscape' in B. Cunliffe and C. Renfrew (eds) *Science and Stonehenge*, Proceedings of the British Academy **92**, 167–202. http://publications.thebritishacademy.ac.uk/pubs/proc/volumes/pba92.html

Davis, S. and Rassmann, K. 2021 'Beyond Newgrange: Brú na Bóinne in the later Neolithic', *Proceedings of the Prehistoric Society* **87**, 189–218. https://doi.org/10.1017/ppr.2021.6

Dietze, M., Kreutzer, S., Fuchs, M. C., Burow, C., Fischer, M. and Schmidt, C. 2013 'A practical guide to the R package Luminescence', *Ancient TL* **32**, 11-18. https://doi.org/10.26034/la.atl.2013.469

Dingwall, K. 2018 'Highway through History – An archaeological journey on the Aberdeen Western Peripheral Route', Edinburgh: Headland Archaeology (UK) Ltd. Còmhdhail Alba/Transport Scotland [website] https://www.transport.gov.scot/media/44074/highway-through-history.pdf [Last accessed: 11 June 2025]

Duller, G.A.T. 2003 'Distinguishing quartz and feldspar in single grain luminescence measurements', *Radiation Measurements* **37**(2), 161-65. https://doi.org/10.1016/S1350-4487(02)00170-1

Ellwood, B.B., Tomkin, J.H., Ratcliffe, K.T., Wright, M. and Kafafy, A.M. 2008 'High-resolution magnetic susceptibility and geochemistry for the Cenomanian/Turonian boundary GSSP with correlation to time equivalent core', *Palaeogeography, Palaeoclimatology, Palaeoecology* **261**(1-2), 105–26. https://doi.org/10.1016/j.palaeo.2008.01.005

Everett, R. and Cribdon, B. 2023 'MetaDamage tool: examining post-mortem damage in sedaDNA on a metagenomic scale', *Frontiers in Ecology and Evolution* **10**, 888421, 1-15. https://doi.org/10.3389/fevo.2022.888421

Exon, S., Gaffney, V., Woodward, A. and Yorston, R. 2001 *Stonehenge Landscapes: Journeys Through Real–And–Imagined Worlds*, Oxford: Archaeopress. [CD published 2000]

Finlay, A., Bates, R., Bensharada, M. and S. Davies 2022 'Applying chemostratigraphic techniques to shallow bore holes: lessons and case studies from Europe's lost frontiers' in V. Gaffney and S. Fitch (eds) *Europe's Lost Frontiers Volume 1 – Context and Methodology*, Oxford, Archaeopress. 137–153. https://doi.org/10.32028/9781803272689

Gaffney, V., Neubauer, W. and Gaffney, C. 2010 'Stonehenge Hidden Landscapes – Project Design' (submitted to the National Trust and English Heritage), University of Birmingham.

Gaffney, C., Gaffney, V., Neubauer, W., Baldwin, E., Chapman, H., Garwood, P., Moulden, H., Sparrow, T., Bates, R., Löcker, K., Hinterleitner, A., Trinks, I., Nau, E., Zitz, T., Flöry, S., Verhoeven, G. and Doneus, M. 2012 'The Stonehenge Hidden Landscapes Project', *Archaeological Prospection* **19**(2), 147–55. https://doi.org/10.1002/arp.1422

Gaffney, V., Fitch, S., Ramsey, E., Yorston, R., Ch'ng. E., Baldwin, E., Bates, R., Gaffney, C., Ruggles, C., Sparrow, T., McMillan, A., Cowley, D., Fraser, S., Murray, C, Murray, H., Hopla, E. and Howard., A 2013 'Time and a place: a lunisolar 'time-reckoner' from 8th millennium BC Scotland', *Internet Archaeology* **34**. http://dx.doi.org/10.11141/ia.34.1

Gaffney, V., Neubauer, W., Garwood, P., Gaffney, C., Löcker, K., Bates, R., De Smedt, P., Baldwin, E., Chapman, H., Hinterleitner, A., Wallner, M., Nau, E., Filzwieser, R., Kainz, J., Trausmuth, T., Schneidhofer, P., Zotti, G., Lugmayer, A., Trinks, I. and Corkum, A. 2018 'Durrington Walls and the Stonehenge Hidden Landscape Project 2010-2016', *Archaeological Prospection* **25**(3), 1–15. https://doi.org/10.1002/arp.1707

Gaffney, V., Baldwin, E., Bates, M., Bates, R., Gaffney, C., Hamilton, D., Kinnaird, T., Neubauer, W., Yorston, R., Allaby, R., Chapman, H., Garwood, P., Löcker, K., Hinterleitner, A., Sparrow, T., Trinks, I., Wallner, M. and Leivers, M. 2020 'A massive, Late Neolithic pit structure associated with Durrington Walls Henge', *Internet Archaeology* **55**. https://doi.org/10.11141/ia.55.4

Gaffney, V., Fitch, S., Bates, M., Ware, R.L., Kinnaird, T., Gearey, B., Hill, T., Telford, R., Batt, C., Stern, B., Whittaker, J., Davies, S., Ben Sharada, M., Everett, R., Cribdon, R., Kistler, L., Harris, S.,Kearney, K., Walker, J., Muru, M., Hamilton, D., Law, M. and Finlay, A. 2020 'Multi-Proxy Characterisation of the Storegga Tsunami and Its Impact on the Early

Holocene Landscapes of the Southern North Sea', *Geosciences* **10**(7), 270. https://doi.org/10.3390/geosciences10070270

Gaffney, V., Gaffney C. and Walker, J. 2023 'Extensive Mesolithic discovery in Bedfordshire shows the importance of pits for understanding early Britain', *The Conversation* [website] https://doi.org/10.64628/AB.hm36mnpd5

Grassé, P.P. 1959 'La reconstruction du nid et les coordinations interindividuelles chez Bellicositermes natalensis et Cubitermes sp. la théorie de la stigmergie: Essai d'interprétation du comportement des termites constructeurs', *Insectes Sociaux* **6**(1), 41–80. https://doi.org/10.1007/BF02223791

Guérin, G., Mercier, N., & Adamiec, G. 2011 'Dose-rate conversion factors: update', *Ancient TL* **29**(1), 5–8. https://doi.org/10.26034/la.atl.2011.443

Guérin, G., Christophe, C., Philippe, A., Murray, A. S., Thomsen, K. J., Tribolo, C., Urbanova, P., Jain, M., Guibert, P., Mercier, N., Kreutzer, S. and Lahaye, C. 2017 'Absorbed dose, equivalent dose, measured dose rates, and implications for OSL age estimates: introducing the Average Dose Model', *Quaternary Geochronology* **41**, 163–73. https://doi.org/10.1016/j.quageo.2017.04.002

Guérin, G., Mercier, N., Nathan R., Adamiec, G., and Lefrais, Y. 2012 'On the use of the infinite matrix assumption and associated concepts: a critical review', *Radiation Measurements* **47**(9), 778–785. https://doi.org/10.1016/j.radmeas.2012.04.004

Helbing, D., Keltsch, J. and Molnar, P. 1997a 'Modelling the evolution of human trail systems', *Nature* **388**, 47–50. https://doi.org/10.1038/40353

Helbing, D., Schweitzer, F., Keltsch, J. and Molna, P. 1997b 'Active walker model for the formation of human and animal trail systems', *Physical Review E* **56**, 2527–39. http://link.aps.org/doi/10.1103/PhysRevE.56.2527

Historic England 2024 'The National Heritage List for England (NHLE) – register of all nationally protected historic buildings and sites in England', *Historic England* [website] https://historicengland.org.uk/listing/the-list/ [Last accessed: 28 May 2025]

Hopson, P., Farrant, A., Newell, A., Marks, R.J., Booth, K., Bateson, L., Woods, M., Wilkinson, I., Brayson, J. and Evans, D. 2006 'Geology of the Salisbury Sheet Area: report on the geology of Sheet 298 Salisbury and its adjacent area. A compilation of the results of the survey in spring and autumn 2003 and from the River Bourne survey of 1999', Internal Report IR/06/011 (unpublished), Nottingham: British Geological Survey. https://nora.nerc.ac.uk/id/eprint/7175

Jarvis, I. and Jarvis, K. E. 1992 'Inductively coupled plasma-atomic emission spectrometry in exploration geochemistry', *Journal of Geochemical Exploration* **44**(1-3), 139-200. https://doi.org/10.1016/0375-6742(92)90050-I

Jarvis, I. and Jarvis, K.E. 1992b 'Plasma spectrometry in the earth sciences: techniques, applications and future trends', *Chemical Geology* **95**, 1–33. https://doi.org/10.1016/0009-2541(92)90041-3

Jeffrey, Z.E., Penn, S., Giles, P.G. and Hastewell, L. 2020 'Identification, investigation and classification of surface depressions and chalk dissolution features using integrated LiDAR and geophysical methods', *Quarterly Journal of Engineering Geology and Hydrogeology* **53**, 620–44. https://doi.org/10.1144/qjegh2019-098

John, B. 2020 'Durrington super-circuit: an hypothesis full of holes', *Stonehenge and the Ice Age* [website] https://brian-mountainman.blogspot.com/2020/06/durrington-super-circuit-hypothesis.html [Last accessed: 4 December 2024]

Kinnaird, T.C., Abellán Santisteban, J., Brandolini, F., Carlton, R., Carrer, F., Civantos, J.M.M., Duggan, M., Holcomb, J.A., Lekakis, S., Ramos Rodríguez, B., Salazar Ortiz, N., Sánchez-Pardo, J.C., Sevara, C., Snyder, J.R., Shillito, L.-M., Silva Sanchez, N., Srivastava, A., Turner, A. and Turner, S. 2025 'Unearthing the histories of agrarian landscapes: a research framework for terraces as sustainable environments', *Geoarchaeology* **40**, e70004. https://doi.org/10.1002/gea.70004

Kinnaird, T.C., Bolòs, J., Turner, A. and Turner, S. 2017a 'Optically-stimulated luminescence profiling and dating of historic agricultural terraces in Catalonia (Spain)', *Journal of Archaeological Science* **78**, 66–77. https://doi.org/10.1016/j.jas.2016.11.003

Kinnaird, T.C., Dawson, T., Sanderson, D.C.W., Hamilton, D., Cresswell, A. and Rennel, R., 2017b. 'Chronostratigraphy of an eroding complex Atlantic round house, Baile Sear, Scotland', *Journal of Coastal and Island Archaeology* **14**(1), 46–60. https://doi.org/10.1080/15564894.2017.1368744

Kircher, M., Sawyer, S., & Meyer, M. 2012 'Double indexing overcomes inaccuracies in multiplex sequencing on the Illumina platform', *Nucleic Acids Research* **40**(1). https://doi.org/10.1093/nar/gkr771

Kolb, T., Tudyka, K., Kadereit, A., Lomax, J., Poreba, G., Zander, A., Zipf, L. and Fuchs, M. 2021 'Data for "The µDose-system: determination of environmental dose rates by combined alpha and beta counting – performance tests and practical experiences"', *JLUpub* [dataset], https://doi.org/10.22029/jlupub-39

Kolb, T., Tudyka, K., Kadereit, A., Lomax, J., Poreba, G., Zander, A., Zipf, L. and Fuchs, M., 2022. 'The µDose system: determination of environmental dose rates by combined alpha and beta counting – performance tests and practical experiences', *Geochronology* **4**, 1–31. https://doi.org/10.5194/gchron-4-1-2022

Kreutzer, S., Burow, C., Dietze, M., Fuchs, M.C., Schmidt, C., Fischer, M., Friedrich, J., Mercier, N., Smedley, R., Christophe, C., Zink, A., Durcan, J.A., King, G.E., Philippe, A., Guérin, G., Riedesel, S., Autzen, M., Guibert, P., Mittelstraß, D., Gray, H.J. and Galharret, J-M. 2024 *Luminescence: Comprehensive Luminescence Dating Data Analysis* https://zenodo.org/records/6345291 [Last accessed: 12 June 2025]

Leivers, M. 2021 'The Army Basing Programme, Stonehenge and the emergence of the Sacred Landscape of Wessex', *Internet Archaeology* **56**. https://doi.org/10.11141/ia.56.2

Leivers, M., Thompson, S., Valdez-Tullett, A. and Wakeham, G. 2020 'Larkhill Service Family Accommodation, Larkhill, Wiltshire Post-excavation Assessment Report', Unpublished report: Wessex Archaeology.

Luke, M. and Kozimiński, M. 2023 'Chapter 4 - Late Mesolithic to Roman land-use at site HRN3486' in M. Luke and D. Shotliff (eds) *Late Mesolithic to Early Anglo-Saxon Land-use at Houghton Regis North, Bedfordshire: Sites HRN3205, HRN3455/6/7, HRN3486 and Woodside Link*, Albion Archaeology Monograph **11**, Bedford: Albion Archaeology. 79–124.

Mejdahl, V. 1979 'Thermoluminescence dating: Beta-dose attenuation in quartz grains', *Archeometry* **29**(1), 61–72. https://doi.org/10.1111/j.1475-4754.1979.tb00241.x

Meyer, M., and Kircher, M. 2010 'Illumina sequencing library preparation for highly multiplexed target capture and sequencing', *Cold Spring Harbor Protocols* **2010**(6), pdb.prot5448. https://doi.org/10.1101/pdb.prot5448

Morris, S. 2024 'Two newly discovered stone circles on Dartmoor boost 'sacred arc' theory', *The Guardian* [website], 15 November 2024. https://www.theguardian.com/science/2024/nov/15/two-newly-discovered-stone-circles-dartmoor-sacred-arc-theory. [Last accessed: 11 September 2025]

Munyikwa, K., Kinnaird, T.C., and Sanderson, D.C.W. 2021 'The potential of portable luminescence readers in geomorphological investigations: a review', *Earth Surface Processes and Landforms* **46**(1), 131–50. https://doi.org/10.1002/esp.4975

Murray, A. S. and Wintle, A. G. 2000 'Luminescence dating of quartz using an improved single-aliquot regenerative-dose protocol', *Radiation Measurements* **32**(1), 57–73. https://doi.org/10.1016/S1350-4487(99)00253-X

Olesik, J.W. 1991 'Elemental analysis using ICP-OES and ICP/MS', *Analytical Chemistry* **63**, 12A-21A. https://doi.org/10.1021/ac00001a711

Parker Pearson, M. and Ramilisonina, 1998 'Stonehenge for the ancestors: the stones pass on the message', *Antiquity* **72**(276), 308–26. https://doi.org/10.1017/S0003598X00086592

Pollard, J. 1995 'Inscribing space: formal deposition at the Later Neolithic monument of Woodhenge, Wiltshire', *Proceedings of the Prehistoric Society* **61**, 137-56. https://doi.org/10.1017/S0079497X00003066

Prescott, J.R. and Hutton, J.T. 1994 'Cosmic ray contributions to dose-rates for luminescence and ESR dating: large depths and long-term time variations', *Radiation Measurements* **23**, 497-500. http://dx.doi.org/10.1016/1350-4487(94)90086-8

Rohland, N. and Reich, D. 2012 'Cost-Effective, High-Throughput DNA Sequencing Libraries for Multiplexed Target Capture', *Genome Research* **22**(5), 939-946. https://doi.org/10.1101/gr.128124.111

Royal Commission On Historical Monuments (England) (RCHME) 1979 *Stonehenge and its Environs: Monuments and Land Use*, Edinburgh: Edinburgh University Press.

Ruggles, C. and Chadburn, A. 2024 'Missing data', *Cosmovisiones/Cosmovisões* **5**, 99-109. https://doi.org/10.24215/26840162e007

Schmidt, A. and Crabb, N. 2017 'Larkhill SFA Haul Road, Larkhill, Wiltshire - Detailed Gradiometer Survey Report', Unpublished report: Wessex Archaeology.

De Smedt, P., Garwood, P., Chapman, H., Deforce, K., De Grave, J., Hanssens, D. and Vandenberghe. D. 2022 'Novel insights into prehistoric land use at Stonehenge by combining electromagnetic and invasive methods with a semi-automated interpretation scheme', *Journal of Archaeological Science* **143**. https://doi.org/10.1016/j.jas.2022.105557

Sperling, C.H.B., Goudie, A.S., Stoddart, D.R. and Poole, G.G. 1977 'Dolines of the Dorset Chalklands and other areas in southern Britain', *Transactions of the Institute of British Geographers* **2**(2), 205-23. https://doi.org/10.2307/621858

Thompson, S. and Powell, A.B. 2018 *Along Prehistoric Lines: Neolithic, Iron Age and Romano-British activity at the former MOD Headquarters, Durrington, Wiltshire*, Oxford: Oxbow Books.

Thorez, J., Bullock, P., Catt, J.A. and Weir, A.H. 1971 'The petrography and origin of deposits filling solution pipes in the Chalk near South Mimms, Hertfordshire', *Geological Magazine* **108**(5), 413-23. https://doi.org/10.1017/S0016756800056454

Tilley C. 1994 *A Phenomenology of Landscape: places, paths, and monuments*, Oxford: Berg.

Tudyka, K., Mi?osz, S., Adamiec, G., Bluszcz, A., Poreba, G., Paszkowski, L. and Kolarczyk, A. 2018 'µDose: A compact system for environmental radioactivity and dose rate measurement', *Radiation Measurements* **118**, 8–13. https://doi.org/10.1016/j.radmeas.2018.07.016

Turner, S., Kinnaird, T., Varinlioglu, G., Emre Şerifoğlu, T., Koparal, E., Demirciler, V. , Athanasoulis, D., Ødegård, K., Crow, J., Jackson, M., Bolòs, J., Sánchez-Pardo, J.C., Carrer, F., Sanderson, D. and Turner, A. 2021 'Agricultural terraces in the Mediterranean: medieval intensification revealed by OSL profiling and dating', *Antiquity* **95**(381), 773–90. https://doi.org/10.15184/aqy.2020.187

Tyler, G. and Jobin Yvon, S. 1995 'ICP-OES, ICP-MS and AAS Techniques Compared', ICP Optical Emission Spectroscopy Technical Note 5, New Jersey: Edison.

Urmston, B. 2014 'Army Rebasing: Larkhill East Site, Salisbury, Wiltshire – Detailed Gradiometer Survey Report', Unpublished report: Wessex Archaeology. https://doi.org/10.5284/1048789

Waltham, T., Bell, F. and Culshaw, M. 2005 *Sinkholes and Subsidence, Karst and Cavernous Rocks in Engineering and Construction*, Heidelberg: Springer Praxis Publishing. https://doi.org/10.1007/b138363

Wolframm-Murray, Y. 2024 'Archaeological strip, map and sample at Parcel 1, Linmere Phase 1 Houghton Regis North 1 Central Bedfordshire Report No. 24/009', Unpublished report, Northampton: Museum of London Archaeology (Mola).

Woodward A.B. and Woodward P.J. 1996 'The Topography of some Barrow Cemeteries in Bronze Age Wessex', *Proceedings of the Prehistoric Society* **62**, 275-291. https://doi.org/10.1017/S0079497X00002814

Worley, F., Madgwick, R., Pelling, R., Marshall, P., Evans, J.A., Lamb, A.L., López-Dóriga, I.L., Bronk Ramsey, C., Dunbar, E., Reimer, P., Vallender, J. and Roberts, D. 2019 'Understanding Middle Neolithic food and farming in and around the Stonehenge World Heritage Site: An integrated approach', *Journal of Archaeological Science: Reports* **26**, 101838. https://doi.org/10.1016/j.jasrep.2019.05.003